

Daniel Stormer Vadseth

Hydrothermal Synthesis of Alkali Niobates

Master's thesis in Materials Science and Engineering

Supervisor: Prof. Mari-Ann Einarsrud

Co-supervisor: Dr. Kenneth Marshall

July 2021



Daniel Stormer Vadseth

Hydrothermal Synthesis of Alkali Niobates

Master's thesis in Materials Science and Engineering
Supervisor: Prof. Mari-Ann Einarsrud
Co-supervisor: Dr. Kenneth Marshall
July 2021

Norwegian University of Science and Technology
Faculty of Natural Sciences
Department of Materials Science and Engineering

Hydrothermal Synthesis of Alkali Niobates

Daniel Stormer Vadseth

21.07.2021

TMT4905 MASTER'S THESIS
SUPERVISOR: Prof. MARI-ANN EINARSRUD
CO-SUPERVISOR: Dr. KENNETH MARSHALL
SPRING 2021

Preface

This report is written as a part of TMT4905 Material Science Master's Thesis. I would like to thank Professor Mari-Ann Einarsrud and Dr. Kenneth Marshall for inspiring and guiding me during this thesis, and for all the help given to me during the time I spent on it. I would also like to thank Angelica Maza Larsen, Iman Yusuf, Henning Dahl, Sean Høiland and Phoebe Lavers for keeping me sane during the completion of this thesis, it would not have been completed without your support.

Abstract

The hydrothermal synthesis conditions of potassium and sodium niobates were investigated with the intention of understanding the effect of synthesis conditions on the reaction kinetics, phase formation, morphology and lattice parameters. Potassium sodium niobate, $K_{0.5}Na_{0.5}NbO_3$ (KNN), has become a contender for the state of the art material lead zirconate-titanate as a piezoelectric material. To understand and improve the properties of KNN it is important to understand potassium niobate, $KNbO_3$, and sodium niobate, $NaNbO_3$, its precursors. This work aims to investigate the hydrothermal synthesis of the $(K, Na)NbO_3$ and other alkali niobate phases made using Nb_2O_5 and $(K, Na)OH$ as precursors and by changing synthesis conditions such as temperature, alkalinity, K:Nb molar ratio, niobium concentration and choice of alkali metal. The samples were analyzed using X-ray diffraction, Raman spectroscopy and scanning electron microscopy to determine the crystallographic structure, local structure and morphology. The results show that the choice of alkali metal as well as higher temperatures and alkalinity are the main factors increasing the reaction kinetics of the $(K, Na)-Nb-O$ system. K:Nb molar ratio affected reaction kinetics as well, as higher K:Nb molar ratio lead to $KNbO_3$ being synthesized at lower pH. Higher K:Nb molar ratio also made the synthesis of monoclinic $KNbO_3$ at temperatures 200 °C and below possible, which has not previously been demonstrated in literature when using Nb_2O_5 as the precursor. Regarding the differences between the alkali metals and their respective niobates, it was found that sodium niobates had faster reaction kinetics and uniform morphology compared to potassium niobates. Potassium niobates showed high degree of agglomeration while sodium niobates did not. Lattice parameters of all $(K, Na)NbO_3$ samples showed that the a and c lattice constants were similar at lower temperatures and deviated at higher temperatures. The β angle of the monoclinic $KNbO_3$ was between 89.9 and 90.1° and approached 90° at higher temperatures. Other niobate phases such as $K_{8-x}H_xNb_6O_{19} \cdot nH_2O$ ($x=0-3$, $n=10, 13, 16$), $K_2Nb_2O_6 \cdot H_2O$, $K_4Nb_6O_{17}$, and $Na_2Nb_2O_6 \cdot H_2O$ were synthesized and analyzed along with the $(K, Na)NbO_3$. $K_2Nb_2O_6 \cdot H_2O$ and $K_4Nb_6O_{17}$ had fiber and nanoplate morphology respectively. The improved understanding of the potassium and sodium niobate systems is another step towards environmentally friendly and cheap piezoelectric materials. The discovery of synthesis conditions that can produce monoclinic $KNbO_3$ using Nb_2O_5 as the precursor instead of metallic niobium powder is a key development towards commercially viable functional potassium niobates.

Sammendrag

Reaksjonsforholdene under hydrotermal syntese av kalium- og natriumniobater har blitt undersøkt med hensikt å forstå effekten av reaksjonsforholdene på kinetikken, faseformasjonen, morfologien og gitterparametrene. Kalium natrium niobat, $K_{0.5}Na_{0.5}NbO_3$ (KNN), har blitt en mulig erstatning for bly zirkonat-titanat (PZT) som et piezoelektrisk material, spesielt for biomedisinske bruksområder. Kunnskap om reaktantene til KNN, kaliumniobat ($KNbO_3$) og natriumniobat ($NaNbO_3$), vil føre til bedre kontroll over dens egenskaper. Dette prosjektet har undersøkt den hydrotermale syntesen av $(K,Na)NbO_3$ og andre alkaliniobater laget med Nb_2O_5 og $(K,Na)OH$ som reaktanter ved å variere synteseparametrene temperatur, alkalinitet, K:Nb molforhold, niobkonsentrasjon og valg av alkalimetall. Produktene fra den hydrotermale syntesen ble analysert med røntgendiffraksjon, Ramanspektroskopi og elektronmikroskop for å undersøke krystallografien, lokalstrukturen og morfologien til alkaliniobatene. Resultatene viser at valg av alkalimetall i tillegg til temperatur og alkalinitet er parametrene med størst påvirkning på reaksjonskinetikken til $(K,Na)-Nb-O$ systemet. K:Nb molforholdet påvirket også reaksjonskinetikken, større K:Nb molforhold førte til syntese av $KNbO_3$ ved lavere KOH konsentrasjoner. Større K:Nb molforhold førte også til syntese av monoklinisk $KNbO_3$ ved temperaturer på 200 °C og lavere, som ikke er demonstrert i litteraturen når Nb_2O_5 er brukt som reaktant. Forskjellen med bruk av kalium og natrium på deres respektive alkaliniobater er at natriumniobatene hadde raskere reaksjonkinetik og mer uniform morfologi i forhold til kaliumniobatene. Kaliumniobatene viste større grad av agglomerasjon, noe natriumniobatene ikke viste. Gitterparametrene til $(K,Na)NbO_3$ viste at gitterkonstantene a og c var tilnærmet like ved lavere temperatur og divergerte ettersom temperaturen økte. β vinkelen i de monokliniske $KNbO_3$ materialene varierte mellom 89.9 og 90.1° og tilnærmet seg 90° ved høyere temperaturer. Andre alkaliniobater enn $(K,Na)NbO_3$, som $K_{8-x}H_xNb_6O_{19} \cdot nH_2O$ ($x=0-3$, $n=10, 13, 16$), $K_2Nb_2O_6 \cdot H_2O$, $K_4Nb_6O_{17}$, og $Na_2Nb_2O_6 \cdot H_2O$, ble også syntetisert. $K_2Nb_2O_6 \cdot H_2O$ hadde fiber morfologi, mens $K_4Nb_6O_{17}$ hadde nanoplate morfologi. Bedre forståelse av kalium- og natriumniobat systemene er nok et steg mot miljøvennlige og billige piezoelektriske materialer. Oppdagelsen av synteseforholdene som fører til dannelse av monoklinisk $KNbO_3$ som bruker Nb_2O_5 som reaktant istedenfor metallisk niob pulver er et viktig steg mot kommersielt tilgjengelige funksjonelle kaliumniobater.

Contents

1	Background	8
1.1	Aim of the Work	10
2	Introduction to Niobium Chemistry	11
2.1	Solution Behavior of Niobium Oxides	11
2.2	Synthesis Parameters and Their Effects on Alkali Niobates	12
2.3	Alkali Niobate Phases And Their Precursor	14
2.3.1	Nb_2O_5	14
2.3.2	$(\text{K,Na})_{8-x}\text{H}_x\text{Nb}_6\text{O}_{19} \cdot n\text{H}_2\text{O}$	14
2.3.3	$\text{K}_4\text{Nb}_6\text{O}_{17}$	16
2.3.4	$(\text{K,Na})_2\text{Nb}_2\text{O}_6 \cdot \text{H}_2\text{O}$	16
2.3.5	$(\text{K,Na})\text{NbO}_3$	16
3	Experimental Methods	19
3.1	Chemicals	19
3.2	Synthesizing Potassium and Sodium Niobates	19
3.2.1	Controlled K:Nb Ratio Experiment Details	20
3.2.2	Constant Niobium Concentration Experiments	20
3.2.3	Sodium Niobium Oxide Synthesis Details	21
3.3	Characterization of the Alkali Niobium Oxides	21
4	Results	23
4.1	Potassium Niobium Oxides XRD Analysis	23
4.1.1	Phase Analysis from the Controlled K:Nb Molar Ratio	24
4.1.2	Phase Analysis from the Constant Niobium Concentration Experiments	25
4.2	Sodium Niobium Oxides	26
4.3	Structure of Potassium Niobates	27
4.3.1	Lattice Parameters of KNbO_3	27
4.3.2	Local Structure of Potassium Niobates	29
4.4	Structure of Sodium Niobates	33
4.4.1	Lattice Parameters of NaNbO_3	33
4.4.2	Local Structure of Sodium Niobates	33
4.5	Morphology of Alkali Niobates	36
5	Discussion	38
5.1	Synthesis Conditions and Their Effects on Alkali Niobates	38
5.1.1	K:Nb Molar Ratio Versus Constant Niobium Concentration	38
5.1.2	Sodium Compared to Potassium on Reaction Kinetics	39
5.2	The Formation of Alkali Niobate Phases	40
5.2.1	Identifying a Low Temperature Low pH Potassium Niobate	40
5.2.2	$\text{K}_4\text{Nb}_6\text{O}_{17}$ Diffractogram and Degree of Hydration	40
5.2.3	Solution Behavior at 5 M KOH	42
5.3	Monoclinic KNbO_3	42

5.4	Formation Mechanisms of Alkali Niobates	44
6	Conclusion	46
7	Future Research	47
8	References	48
	Appendix	54
A	X-Ray Diffraction Patterns	54
B	Raman Spectroscopy	57

List of Abbreviation

Abbreviation	Explanation
PZT	Lead Zirconate-Titanate
MPB	Morphotropic Phase Boundary
KNN	Potassium Sodium Niobate ($K_{0.5}Na_{0.5}NbO_3$)
XRD	X-Ray Diffraction
POM	Polyoxometalate
PONb	Polyoxoniobate
T-Nb ₂ O ₅	Orthorhombic Niobium Oxide
SEM	Scanning Electron Microscopy
FEG	Field Emission electron Gun
EM	Electromagnetic
RT	Room Temperature
COD	Crystallography Open Database
SOMS	Sandia Octahedral Molecular Sieve

1 Background

Materials are becoming more complex to deal with increasingly advanced technological demands in today's society. Materials today employ more complex synthesis methods and use more dopants, rare earth elements and critical materials than they did less than 40 years ago [1]. The list of elements required to produce a personal phone have doubled since the 1980's where a Motorola DynaTAC 8000X needed around 35 elements. A 2018 smartphone doubles that, needing between 65 and 70 elements which is almost every stable element in the periodic table. Despite new technologies improving the lives of billions of people, the trend is worrying as this increased complexity comes with several challenges: all elements need to be mined somewhere, supply-chain risks are multiplied with more elements added, recycling and disposal becomes more difficult as dopants are added and high energy synthesis increases the overall carbon footprint.

Nature however has shown that something as complex as life itself can be created using less than 30 elements [1]. Complex functions do not necessarily require more dopants, critical materials, rare earth elements and complex synthesis methods, nature manages without. Bones and wood are examples of piezoelectric materials [2] that have been known for more than half a century and chlorophyll converts solar power to chemical energy, all at basically room temperature. In nature there is no permanent waste; everything is part of natural cycles that take waste from one process and use it as feed for another. If material scientists could emulate nature and create recyclable materials using less dopants and less energy, a whole new era of sustainability in the material science world would begin. This paradigm has been dubbed 'green chemistry'.

Now what if you were told there is an element in the periodic table with all kinds of amazing physical and chemical properties with a wide range of applications. This element works well in paint and solder, protects machinery from wear and tear, is great in rechargeable batteries, used in efficient thin film solar cell material and makes state of the art piezoelectric ceramics. This element is abundant and inexpensive. It may appear that this element is the "potato" of inorganic chemistry, useful in many different forms and used everywhere. While most people have heard of this element, it is certainly not widely celebrated. This element is number 82 in the periodic table, lead. The many benefits of lead and its compounds have long been known but in recent human history the long term cost on human health and the environment from the use of these compounds has been discovered [3,4]. Throughout the 1990's and onward, lead has been removed from many facets of society. A few notable exceptions are lead acid batteries, lead-containing piezoelectric components and some types of solder which still contain lead today. Otherwise the use of lead based materials are heavily restricted or outright banned for many applications.

Lead is very hard to eliminate from certain functional materials such as lead zirconate titanate (PZT). PZT is a state of the art material with excellent piezoelectric properties over a broad temperature range, meaning it is still in use today despite the environmental and health concerns. The properties that make PZT such a useful material are the superior piezoelectric coefficient, dielectric

constant and electromechanical coupling coefficient [5]. One important reason properties are superior is because of the systems ease of polarizability brought on by the composition being at a morphotropic phase boundary (MPB). Piezoelectric materials are important to many technologies such as bioactive materials [6], energy harvesters [7], sensors, actuators [8] and transducers [9]. Since piezoelectric materials are used in more and more applications as new uses are researched and scaled up developing lead-free alternatives is very important.

How can PZT be replaced by a lead free piezoelectric alternative without compromising on quality? The material qualifications required for advanced modern technology are extensive. The key properties for a piezoelectric material are high piezoelectric coefficient, good electromechanical coupling, low permittivity, good stability and high enough Curie temperature in the desired temperature range [5]. The exact material properties necessary depend on the specific application, but these are some of the important benchmarks to consider. A lead-free contender to PZT would need to function well in these categories because a major downside means the material simply does not function well enough for most applications. Another important factor to consider is that a lead-free replacement needs to be environmentally friendly and non-toxic. With this list of qualifications in mind, the list of viable replacement materials becomes narrow, and a few categories stand out. Potassium sodium niobates ($K_{1-x}Na_xNbO_3$, $x=0-1$), barium titanates and sodium bismuth titanates are three general material categories that can fit the criteria for a lead-free piezoelectric material. To optimize properties of these materials several variations such as doping and stoichiometry make the materials in these broader categories better suited for specific applications.

Niobium is a group V element that has great potential in replacing lead-containing piezoelectric materials. Niobium is non-toxic and environmentally friendly, abundant and possesses a lot of interesting chemical properties as will be further examined in a later section. Niobium oxides have a pH dependence in structural composition, in alkaline conditions it assembles into NbO_6 octahedral structures spontaneously [10, 11]. The octahedra form a cluster called the Lindqvist anion ($[Nb_6O_{19}]^{8-}$) with six of these octahedra as building blocks. These hexaniobates can then act as a starting point for many new niobium-based compounds such as alkali perovskites. Alkali perovskites ($ANbO_3$, $A=Li,Na,K,Rb$) have long been known to have functional properties such as piezo- and ferroelectricity. A more sustainable method of production, non toxicity, abundance and low price are some of the reasons potassium sodium niobates, specifically $K_{0.5}Na_{0.5}NbO_3$ (KNN), has become one of the most promising replacements for PZT for certain uses, and has been researched extensively the past two decades [12]. A problem with niobium is that the mining mainly happens in Brazil. Mining in Brazil comes with issues such as deforestation, lack of environmental regulation and workers conditions. Although large ore deposits are found in Brazil, these problems can be addressed and mining can be done other places such as Australia.

Hydrothermal synthesis is the sustainable method that adds to the

competitive edge of KNN. Hydrothermal synthesis is a versatile wet-chemical method that uses water at temperatures between 100 and 400 °C to create highly crystalline functional materials. Solvothermal synthesis use the same principles as hydrothermal synthesis but with a solvent different from pure water. To achieve temperatures of the solvent above the atmospheric boiling point the liquid and the precursors are put into an autoclave which is sealed to withstand high pressure. At high pressure, the boiling point of water is elevated and the system can be in the liquid phase at high temperatures. The properties of water, such as the dielectric constant, changes under high pressure and temperature. The changes to the properties of water changes the solubility, which also causes higher reactivity. All these factors combined make hydrothermal synthesis a great method of producing functional materials, and using low temperatures and water as the solvent makes it environmentally favorable.

1.1 Aim of the Work

The aim of the thesis is the exploration of hydrothermal synthesis of potassium and sodium niobates. The points of interest that were investigated are:

- The effect of alkalinity and temperature on the type of alkali niobate product
- The effect of the type of alkali metal cation on reaction kinetics
- The effect of niobium concentration and K:Nb molar ratio on the hydrothermal synthesis of potassium niobates
- How crystallite size and lattice parameters are affected by the different parameters varied

The theory section delves into the chemistry of niobium and niobate phases. Knowledge of the chemistry behind niobium and hydrothermal synthesis is vital. With a solid understanding of the theory, the results from the research can be interpreted and correlations can be explained. Understanding the alkali niobate system is vital for controlling the properties of the materials, ultimately leading to an expansion of the functional material engineering toolbox.

2 Introduction to Niobium Chemistry

Polyoxometalates (POMs) are anionic metal-oxo clusters, the metals being transition metals from group V and VI. The most common metals studied are Mo, W and V as well as Nb and Ta more recently. Alkali niobium oxides have been known for decades but have seen more research since the early 2000's [13]. Up until the 21st century the known PONbs were the hexaniobate anion $[\text{Nb}_6\text{O}_{19}]^{8-}$, some related coordination complexes such as $\text{Mn}[\text{Nb}_6\text{O}_{19}]_2^{12-}$ and one report of a larger decaniobate structure ($[\text{Nb}_{10}\text{O}_{28}]^{6-}$) [13]. In the past two decades the research has continued to discover new polyoxoniobate (POM) structures and found answers to questions about their chemistry. PONbs, as well as other POMs, have the ability to form a large variety of structures in solution and in solid state. The versatility of niobium chemistry and the broad spectrum of niobium based materials have made the understanding of the system more and more important. Understanding leads to control of the synthesis, enabling the synthesis of a wide array of new materials to scientists and engineers the world over. One of the most interesting alkali niobates is potassium sodium niobate ($\text{K}_{0.5}\text{Na}_{0.5}\text{NbO}_3$), due to its dielectric and piezoelectric properties along with biocompatibility. Better understanding the K-Na-Nb-O system and its precursors will have important implications, especially for biomedical materials [12].

2.1 Solution Behavior of Niobium Oxides

One of the reasons PONbs have such rich diversity of structures is their behavior in solution and their structural dependence on pH [14, 15]. pH is an easy parameter to independently vary and has a large impact on the niobium oxide cluster geometry. Varying the pH can also introduce vacancies in the clusters [16], which is an important design tool for material chemists. These vacancies can be filled with most other cationic metals which opens up possibilities for new structures and complexes of PONbs as well as introducing new functionalities. Filling these vacancies can introduce functional properties such as catalytic behavior, rich redox activity and more.

PONbs are often soluble in aqueous solutions but can be precipitated reversibly and transferred into non-aqueous phases intact. Ethanol is an example of a non-aqueous solvent that can be used to precipitate out crystalline alkali niobates with a variety of interesting crystal structures and morphology [17]. With a rich solution chemistry PONbs can be synthesized at low temperatures using hydrothermal or solvothermal synthesis. Due to the fact that most PONbs are stabilized in solution traditional ceramic synthesis methods cannot be used to the same effect [13].

Hydrothermal synthesis plays an important role in the richness and success with PONb chemistry. The early reports of alkali niobate synthesis used an alkali hydroxide melt with solid Nb_2O_5 making it a solid state reaction where results were hard to reproduce [18]. Hydrothermal synthesis leads to reproducible results with better control over the synthesis parameters and results. This low energy synthesis method has made new niobium discoveries possible due to the increased control of stoichiometry, morphology and geometry [19, 20]. This method functions at low temperatures compared to traditional ceramic synthesis methods, such as

pellet sintering, because of the increased reactivity under hydrothermal conditions. A problem with hydrothermal synthesis comes with the scalability of the method. When increasing the size of the reactor in batch mode, heat transfer is significantly hindered [21]. However, flow reactors are a possible solution to this problem.

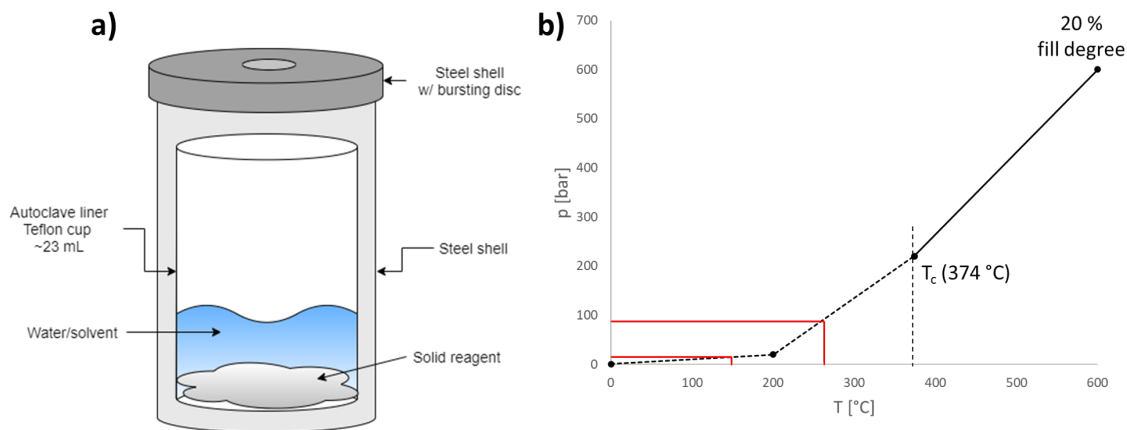


Figure 2.1: a) A schematic of the autoclave setup with the autoclave liner, steel shell and lid, water or solvent and the solid reagents. The lid is equipped with a bursting disc for safety. b) The figure shows pressure inside the autoclave as a function of temperature for hydrothermal synthesis with a pure water solvent, T_c being the critical temperature of water. The red lines indicate the pressure range from approximately 10 bar at 150 °C to about 100 bar at 240 °C. The graph, adopted from [22], is dependent on the filling factor. Here the graph for a fill factor of 20 % is shown, higher filling factor leads to higher pressure.

2.2 Synthesis Parameters and Their Effects on Alkali Niobates

When considering the hydrothermal reaction between Nb_2O_5 and $(\text{K}, \text{Na})\text{OH}$ to form different alkali niobate phases, several synthesis parameters are important. Synthesis parameters such as temperature, alkalinity, time and concentration of precursors affect the reaction and the products. The different parameters can also change the solution chemistry, and can increase or decrease solubility for the different alkali niobates which changes stability.

Temperature is one of the most important factors in the hydrothermal synthesis of alkali niobates, as well as affecting particle size. Higher temperature means more energy added to the system, and with enough energy the system surmounts the energy barrier and can react. Increased temperature also changes the properties of the solvent as well, e.g. rapidly decreasing the dielectric constant for water approaching that of a non-polar solvent. As the temperature increases the solvent evaporates and the gas expands, increasing the pressure. The high pressure allows the liquid solvent to be stable as a liquid above the regular boiling point. This increases the energy in the system and leads to solvent conditions that are favorable for reaction [19]. A study investigating the effect of 4 factors [23],

temperature, stirring speed, molar ratio and time, reaction temperature had the biggest impact on dissolution of Nb₂O₅. Once dissolved, Nb₂O₅ rapidly forms K_{8-x}H_xNb₆O₁₉ · nH₂O (x=0-3) which goes on to further react into other alkali niobates.

Alkalinity is a factor that plays a role in both the reaction kinetics and the stability of phases after synthesis. With different pH and temperature the predominant phase can be selected [17, 24]. With increased alkalinity the stability and reaction kinetics of ANbO₃ (A=Li,Na,K,Rb,Cs) are increased. Decreasing alkalinity increases the stability of other phases such as the hexaniobate Lindqvist anion phase A_{8-x}H_xNb₆O₁₉ · nH₂O [25, 26]. Alkalinity can also have an effect on the morphology for certain phases [25].

Reaction time affects whether the reaction reaches completion or not, although the reaction kinetics are far more important. Crystallite size, up until a certain point, is also affected by the time [27]. Reaction kinetics are affected by other factors such as which temperature, pH and alkali metal is used. In multi-step reactions with one or more intermediate species, the reaction time needed to reach the final product of the reaction (e.g. (K,Na)NbO₃) varies depending on temperature and (K,Na)OH concentration. Shorter time at the hydrothermal synthesis temperature can lead to these intermediate phases (e.g. Na₂Nb₂O₆ · H₂O) being present [25, 28]. Most alkali niobate reactions will reach completion in a short time, because the reaction kinetics are fast. The reaction between NaOH and Nb₂O₅ to form NaNbO₃ was studied *in situ* with a sapphire capillary the took between 8 seconds and 7 minutes depending on the NaOH concentration and temperature [29].

The effect of the molar ratio between the different species plays a role for some alkali niobates. Although the effect of (K,Na):Nb molar ratio is not specifically reported on as much in the literature for the synthesis of simple A-Nb phases, higher concentration of reactants increases the driving force during reaction. For the synthesis of KNN (K_{1-x}Na_xNbO₃, x=0-1) the K:Na ratio during synthesis is vitally important for the structure and properties of the final product. For some larger alkali niobate structures the (K,Na,Li):Nb ratio plays a role in the final geometry and stoichiometry [13, 30].

Solvothermal synthesis has a big effect on reaction kinetics, morphology and phase composition [17, 24]. Adding a different solvent, e.g. an ethanol and water solution, to the autoclave changes the chemical properties of the solvent such as the dielectric constant and vapor pressure. These changes are compounded when the temperature and pressure increase during synthesis. The stability of intermediate phases changes depending on the solvent. Stable intermediate phases means they can more easily react into new phases before decomposing.

Concentrations of the precursors have an effect on the reaction rates and the driving forces for chemical reaction. In the reaction between Nb₂O₅ and (K,Na)OH to form (K,Na)NbO₃, higher niobium concentration and (K,Na)OH concentration increases the driving force. When considering thermodynamics, the "driving force" can be expressed as

$$\Delta_r G^\circ = -RT \ln(K) \quad (1)$$

where $\Delta_r G$ is the Gibbs free energy, R is the gas constant, T is temperature and K is the equilibrium constant [31]. Equation 1 describes the Gibbs free energy for a reaction at equilibrium, for reactions at non-equilibrium the reaction quotient Q is used. Concentration is included in the equilibrium constant K and reaction quotient Q , which are described as

$$K = \frac{\text{activity of products}}{\text{activity of reactants}} = \frac{a_{\text{prod}}}{a_{\text{react}}}, (a_i = c_i \gamma_i) \quad (2)$$

for both of these factors. Activity of species i can be described as the concentration of the species multiplied by the activity coefficient γ as equation 2 describes. Combining all the equations gives a relationship between the driving force and the concentration of species. This relation can be simplified and expressed as

$$\Delta_r G^\circ \propto \ln\left(\frac{c_{\text{prod}}}{c_{\text{react}}}\right) \quad (3)$$

for a system in equilibrium. If ΔG is negative the reaction is spontaneous. Higher concentration of reactants make the logarithmic term smaller, leading to a higher driving force for reaction. This is a simplification of the thermodynamic considerations and does not take kinetics into account, but the general relation between ΔG and the concentrations is important.

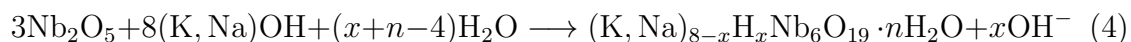
2.3 Alkali Niobate Phases And Their Precursor

2.3.1 Nb_2O_5

While not an *alkali* niobate, the structure of the precursor in the reactions to all the alkali niobates is important. Orthorhombic Nb_2O_5 (T- Nb_2O_5) consists of strongly distorted NbO_6 octahedra and NbO_7 pentagonal dipyramids. The unit cell has consists of 16.8 niobium atoms and 42 oxygen atoms, where the 0.8 niobium atoms come from partially filled niobium sites [32]. With sufficiently high pH the Nb_2O_5 dissolves when H_2O and K^+/Na^+ moves into the structure [23]. Bonds break and form $[\text{NbO}_6]^{7-}$ octahedra in solution which can further react to form alkali niobates. Crystal water helps screen the charges of the niobium oxygen octahedra, allowing edge shared structures to form [29].

2.3.2 $(\text{K}, \text{Na})_{8-x}\text{H}_x\text{Nb}_6\text{O}_{19} \cdot n\text{H}_2\text{O}$

The niobium oxygen octahedra ($[\text{NbO}_6]^{7-}$) in solution quickly react to form the $[\text{Nb}_6\text{O}_{19}]^{8-}$ which is described by the chemical reaction



where the first step is dissolution of Nb_2O_5 . The dissolved Nb_2O_5 forms $[\text{NbO}_6]^{7-}$ octahedra that assemble into $[\text{Nb}_6\text{O}_{19}]^{8-}$ Lindqvist anion upon heating. The $[\text{Nb}_6\text{O}_{19}]^{8-}$ Lindqvist anion in solution can precipitate into

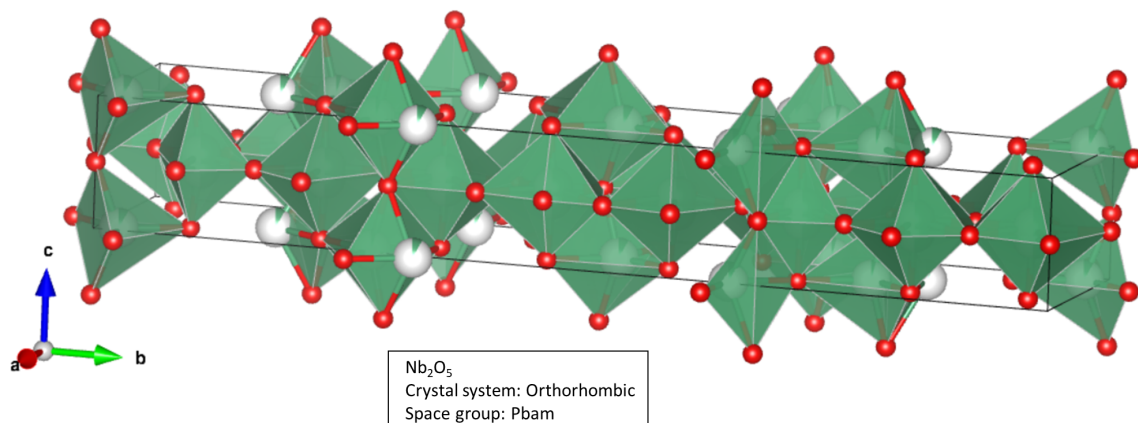


Figure 2.2: The unit cell of orthorhombic Nb_2O_5 (T- Nb_2O_5). Nb_2O_5 contains octahedra (NbO_6), tetrahedra (NbO_4) and pentagonal dipyramid decahedra (NbO_7). The occupancy of some sites are less than 1, which is shown as partially colored in spheres with 50 %, 8 % or 4 % green. Niobium is shown in green, oxygen in red.

$(\text{K}, \text{Na})_{8-x}\text{H}_x\text{Nb}_6\text{O}_{19} \cdot n\text{H}_2\text{O}$ ($x=0-3$, $n=10-16$) or break up into smaller fragments of $[\text{NbO}_6]^{7-}$ [17, 27]. The hexaniobate Lindqvist anion has the highest charge density among the POMs [33]. The potassium and sodium hexaniobates are well hydrated, with between 10 and 16 crystal water per unit cell to screen the charge. Sodium and potassium hexaniobate are very similar materials, the main differences being the amount of crystal water and the orientation and placement of the Lindqvist anions in relation to each other and to the potassium or sodium. The difference between two potassium hexaniobates, where the difference is the amount of crystal water, are shown in figure 2.3.

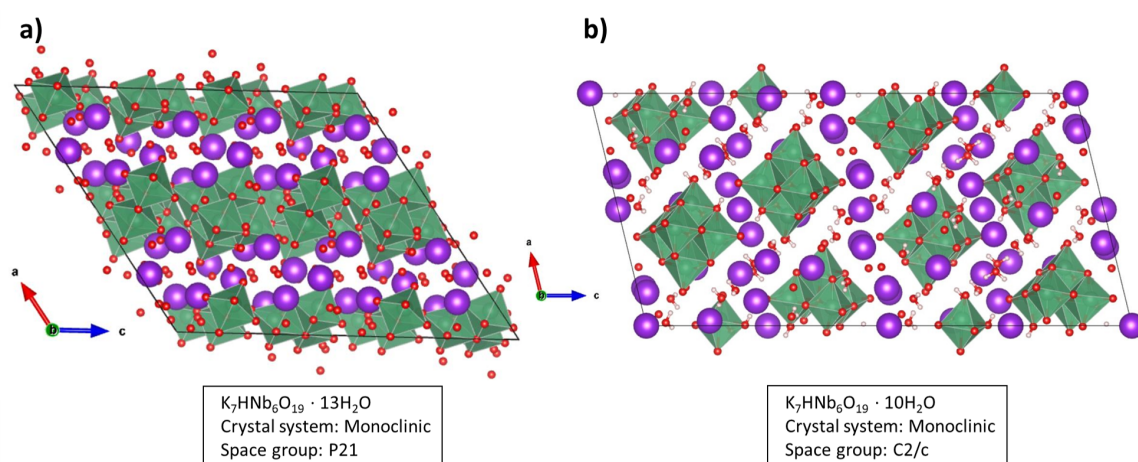


Figure 2.3: Unit cells of two hydrated potassium hexaniobate phases, a) $\text{K}_7\text{HNB}_6\text{O}_{19} \cdot 13\text{H}_2\text{O}$ and b) $\text{K}_7\text{HNB}_6\text{O}_{19} \cdot 10\text{H}_2\text{O}$. The phases are viewed straight down the b -axis to show the potassium layers among the hexaniobate clusters.

2.3.3 $K_4Nb_6O_{17}$

$K_4Nb_6O_{17}$ is a hexaniobate phase comprised of $[NbO_6]^{7-}$ octahedra grouped in clusters of 6. These 6 octahedra are edge shared, though not in the same configuration as the Lindqvist anion where all the octahedra are centered around a central oxygen atom. Each $[Nb_6O_{17}]^{4-}$ unit is corner shared with its neighboring units forming niobium oxide layers with potassium layers in between. $K_7Nb_6O_{17}$ has different degrees of hydration, from dehydrated $K_4Nb_6O_{17}$ to the more hydrated forms such as $K_4Nb_6O_{17} \cdot 3H_2O$ and $K_4Nb_6O_{17} \cdot 4.5H_2O$. Research has shown $K_4Nb_6O_{17}$ can be used for leaching of radioactive cations from solution [34] and has photocatalytic water splitting capabilities [35].

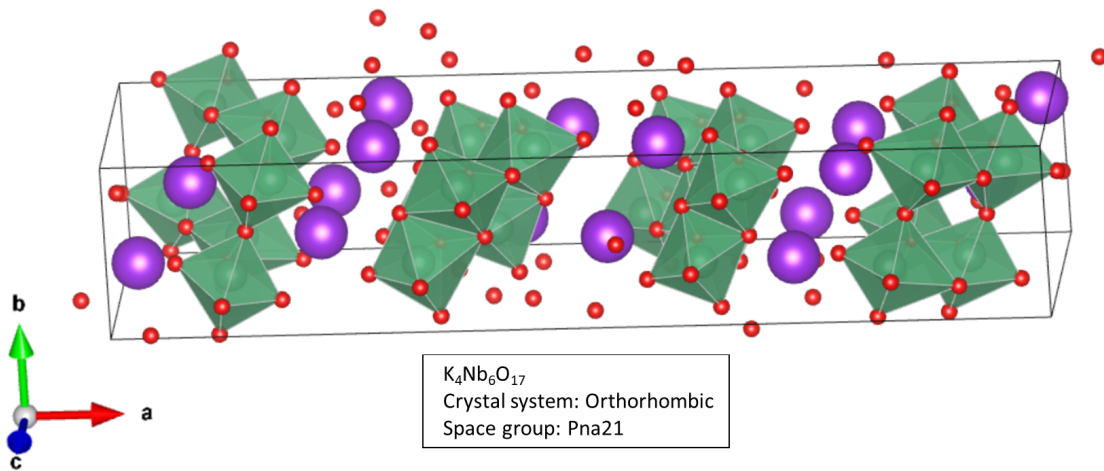


Figure 2.4: Unit cell of $K_4Nb_6O_{17}$ which consists of niobium and oxygen (green and red respectively) octahedra with potassium (purple) layers in between.

2.3.4 $(K,Na)_2Nb_2O_6 \cdot H_2O$

$(K,Na)_2Nb_2O_6 \cdot H_2O$ is a phase consisting of edge shared octahedra chains along the b -axis as seen in figure 2.5. Along the a -axis are $(K,Na)O_6$ octahedra layers, and between the NbO_6 chains are tunnels half filled with K^+/Na^+ . This structure is called the sandia octahedral molecular sieve (SOMS) structure. For both sodium and potassium this phase grows preferentially in the (020) direction which runs along the chains and the b -axis. This creates crystals with a nano- to microfiber morphology and half filled tunnel structure along the fibers [17, 36]. Both $Na_2Nb_2O_6 \cdot H_2O$ and $K_2Nb_2O_6 \cdot H_2O$ are metastable phases, but with sodium this phase is more stable. $K_2Nb_2O_6$ has also recently been reported with a pyrochlore type cubic structure with photocatalytic properties [37, 38].

2.3.5 $(K,Na)NbO_3$

$(K,Na)NbO_3$ is a material with a perovskite ABO_3 structure with interesting non-linear optical, photocatalytic, ferroelectric and piezoelectric properties [39, 40]. The orthorhombic structure is the most stable $KNbO_3$ phase at room temperature. Below

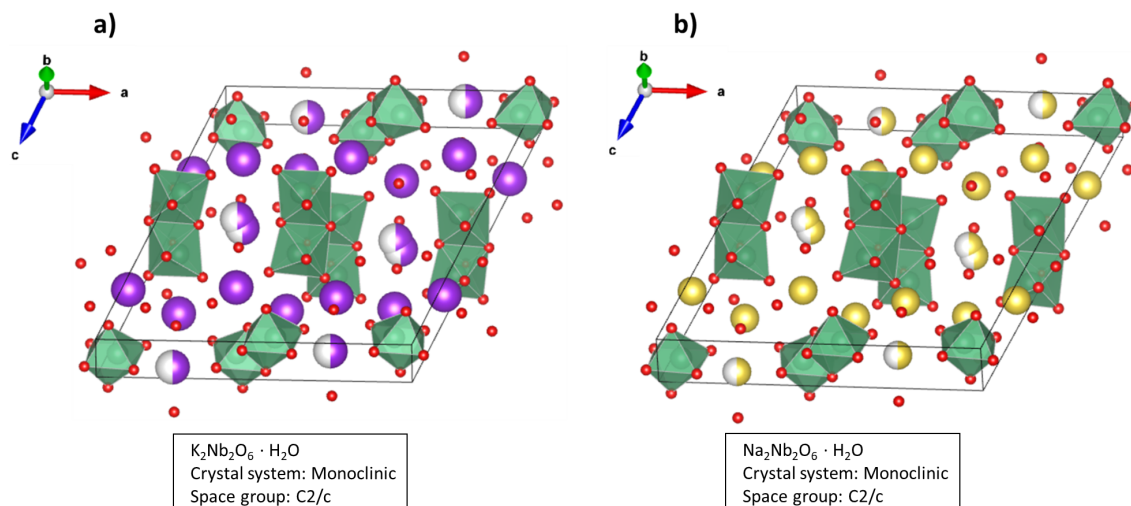


Figure 2.5: Unit cells of **a)** $K_2Nb_2O_6 \cdot H_2O$ and **b)** $Na_2Nb_2O_6 \cdot H_2O$. The niobium (green) and the oxygen (red) form octahedra that stack on top of each other in long chains, while the potassium (purple) or sodium (yellow) fill the channels between. The half filled spheres show which atoms have occupancy of 0.5.

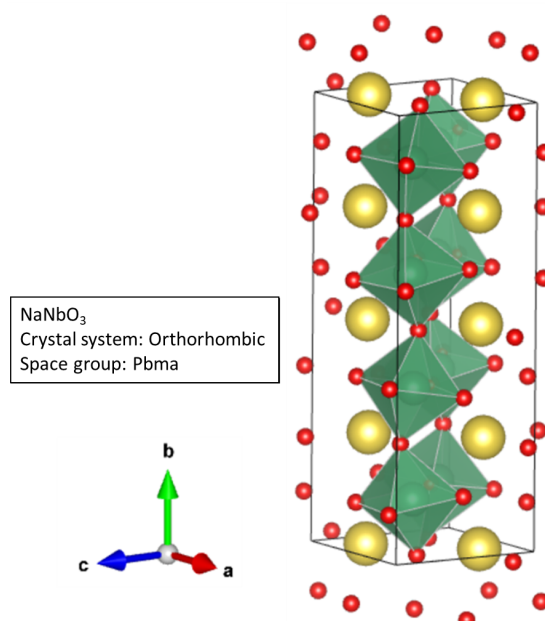


Figure 2.6: Unit cell of orthorhombic $NaNbO_3$. The tilted octahedra consist of niobium (green) surrounded by oxygen (red) with sodium (yellow) interlaced in the structure.

-10 °C (263 K) the most stable crystal structure is rhombohedral. Above -10 °C the rhombohedral structure changes to orthorhombic, which is the most stable structure up until 224 °C (497 K), above which the most stable structure is tetragonal. The tetragonal structure is stable up to 437 °C (710 K) where the most stable crystal structure becomes cubic $KNbO_3$ [27, 41].

Monoclinic $KNbO_3$ is a metastable phase. The monoclinic $KNbO_3$ phase differs

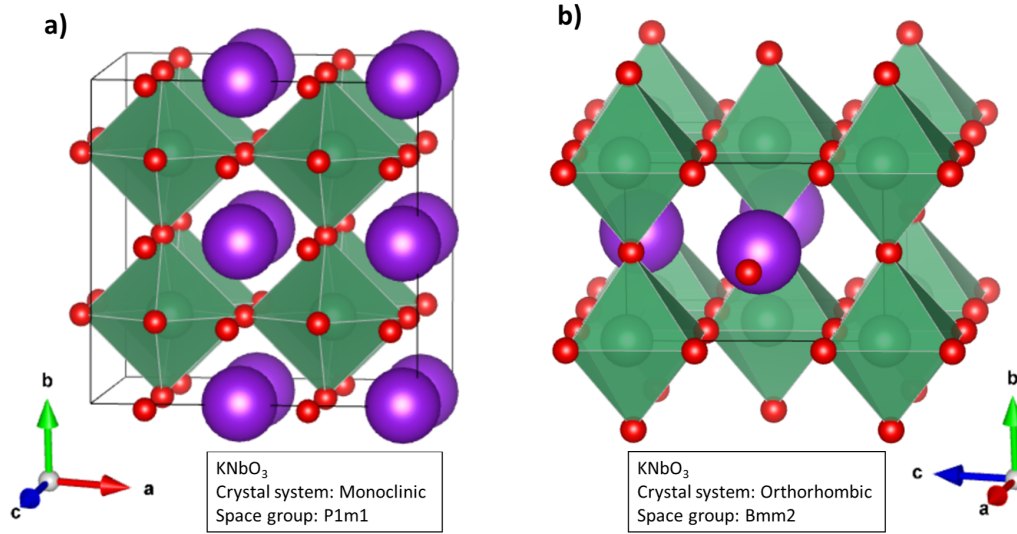


Figure 2.7: Enlarged unit cells of **a)** Monoclinic KNbO_3 and **b)** Orthorhombic KNbO_3 . The monoclinic phase has a β angle (between the a and c axis) close but not equal to 90° . Niobium is shown in green, oxygen in red and potassium in purple.

from the orthorhombic phase by a slight deviations from 90° β angle of the unit cell by around 0.10° [40]. This metastable monoclinic phase has been produced using metallic niobium powder and KOH [40] with hydrothermal synthesis, by liquid phase epitaxy from a K_2CO_3 and Nb_2O_5 melt on a SrTiO_3 substrate [42] and other methods. Synthesis of monoclinic KNbO_3 using hydrothermal methods with the precursor Nb_2O_5 alone has not yet been demonstrated in literature.

3 Experimental Methods

3.1 Chemicals

Table 3.1: Information on the chemicals used to make the precursors and the solutions used in this project.

Chemical	Molecular formula	Purity [%]	Supplier
Ammonium niobium (V) oxalate	$\text{NH}_4\text{NbO}(\text{C}_2\text{O}_4)_2 \cdot x\text{H}_2\text{O}$	99.99	Sigma-Aldrich
Ammonium solution	$\text{NH}_3, (\text{diss.})$	28	Sigma-Aldrich
Potassium hydroxide	KOH	90	Sigma-Aldrich
Sodium hydroxide	NaOH	97	Sigma-Aldrich

Niobic acid was prepared as partly described by Mokkelbost *et al.* by mixing ammonium niobium (V) oxalate (60.0 g) in 700 mL distilled water. The solution was stirred for 24 hours on a hotplate at 60 °C until the solution became clear [43]. Ammonium solution (1%, 125 mL) was added precipitating niobic acid ($\text{Nb}_2\text{O}_5 \cdot x\text{H}_2\text{O}$). After another 72 hours of stirring at room temperature the solution was centrifuged and washed with three times with the 1 % ammonium solution to get rid of the oxalate. T- Nb_2O_5 was prepared from this niobic acid by evaporation of the solution in an open crystallization beaker at 60 °C under stirring. The dried product was calcined at 500 °C for 10 hours with a 2.5 hour heating time and cooled in air. This gave orthorhombic Nb_2O_5 (T- Nb_2O_5) as confirmed by XRD analysis.

A 10.00(8) $\frac{\text{mol}}{\text{L}}$ potassium hydroxide solution was prepared by mixing KOH (155.874(12) g) with water (250.00(15) mL, distilled). KOH solutions of 7.50(8) M, 5.00(5) M, 2.50(3) M and 1.0(2) M were prepared by dilution of the 10 M stock solution. All uncertainties were calculated using Gaussian error propagation and are given in the parentheses.

3.2 Synthesizing Potassium and Sodium Niobates

The hydrothermal synthesis process, described in figure 3.1, used a steel shell autoclave with a 23 mL Teflon autoclave liner as seen in figure 2.1. First, Nb_2O_5 and (K,Na)OH were mixed together in an autoclave, the autoclave was heated to the desired temperature for 18 hours. After heating the autoclave was cooled in RT and washed and filtered with 96 % ethanol using a Büchner funnel. This removed water and KOH from the solid product and precipitated free niobate species in solution, if any. Some samples contained only soluble alkali niobates (such as for example $\text{K}_{8-x}\text{H}_x\text{Nb}_6\text{O}_{19} \cdot n\text{H}_2\text{O}$) and contained no solid product. These solutions, whether transparent or opaque, were crystallized in a beaker using ethanol before filtering and ethanol washing.

To investigate the effects of different parameters three different experiment series were planned, varying the K:Nb ratio, niobium concentration and choice of

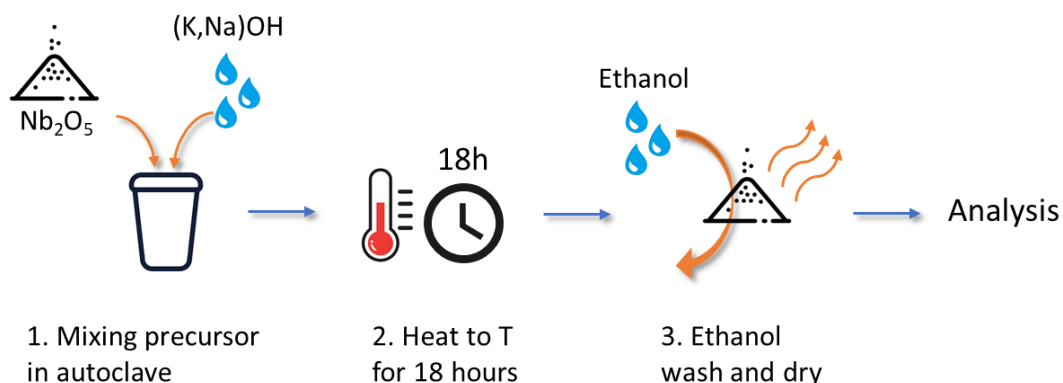


Figure 3.1: Schematic representation of the synthesis method of alkali niobates. First, Nb_2O_5 and $(\text{K,Na})\text{OH}$ were mixed together in an autoclave(1), the autoclave was heated to the desired temperature for 18 hours(2). The crystalline product from the hydrothermal synthesis was washed with ethanol and dried(3) before the final product was analyzed and characterized.

alkali metal. The reaction time for all the experiments were 18 hours, and the autoclaves were cooled in air at RT for about 2 hours before filtering. To control the K:Nb ratio and niobium concentration, the volume of KOH varied between 1 and 5 mL. The nomenclature of the different samples follow the general format of (Experiment series)-[KOH]-Temperature, e.g. K:Nb-10-150 (K:Nb experiment, 10 M KOH, 150 °C).

3.2.1 Controlled K:Nb Ratio Experiment Details

The molar ratio between potassium and niobium (K:Nb molar ratio) was controlled, not kept fully constant, at between 1.33 and 2.66. Compared to the [Nb] experiment series, the molar ratios and excess potassium for the K:Nb experiments are lower. Excess potassium means the limiting reactant is always niobium. The volume varied between 1 and 5 mL to maintain 1.33 or more K:Nb molar ratio. Niobium concentrations varied with the volume, between 0.752 and 3.76 M, as is detailed in table 3.2.

3.2.2 Constant Niobium Concentration Experiments

The volume and weight of added Nb_2O_5 remained constant giving a constant [Nb] in the solution. Each of the parameters for the constant niobium experiments are detailed in table 3.3. In these experiments the niobium concentration was kept constant at 0.752 M while the K:Nb molar ratio varied between 6.65 and 13.3 depending on the KOH concentration. The volume of solution was kept constant at 5 mL for all the experiments. These experiments investigated more temperatures between 150-200 °C compared to the K:Nb molar ratio and the sodium experiments.

Table 3.2: The parameters of the controlled K:Nb experiments. The temperature and KOH concentration is shown in the "experiment name" column, where the name of the experiment details this as follows: (experiment name)-[KOH]-temperature. The weight of niobium added to all the experiments was 0.5000(6) g. The shaded rows separate the different KOH concentrations.

Experiment name "Exp-[KOH]-T"	Volume KOH [mL]	[Nb] [$\frac{mol}{L}$]	K:Nb molar ratio
K:Nb-10-150	1	3.76	2.66
K:Nb-10-200	1	3.76	2.66
K:Nb-10-240	1	3.76	2.66
K:Nb-7.5-150	1	3.76	1.99
K:Nb-7.5-200	1	3.76	1.99
K:Nb-7.5-240	1	3.76	1.99
K:Nb-5-150	1	3.76	1.33
K:Nb-5-200	1	3.76	1.33
K:Nb-5-240	1	3.76	1.33
K:Nb-2.5-150	2	1.88	1.33
K:Nb-2.5-200	2	1.88	1.33
K:Nb-2.5-240	2	1.88	1.33
K:Nb-1-150	5	0.752	1.33
K:Nb-1-200	5	0.752	1.33
K:Nb-1-240	5	0.752	1.33

3.2.3 Sodium Niobium Oxide Synthesis Details

The synthesis parameters for the experiments where sodium hydroxide was used are detailed in table 3.4. The volume of NaOH was 1 mL for all the sodium experiments, same as for the 7.5 M and 10 M controlled K:Nb molar ratio experiments. The Niobium concentration was 3.76 and the Na:Nb molar ratio was between 1.99 and 2.66.

3.3 Characterization of the Alkali Niobium Oxides

The Raman spectra were acquired using a Witec Alpha 300r to get information on the local structure in the samples, with a resolution of 4 cm^{-1} . The X-ray diffractograms were recorded using a Bruker D8 ADVANCE DaVinci. The XRD analysis was used to determine which phases were present and structural information of these phases. The samples were scanned with a 2 angle from 5-75 $^{\circ}$ for 1 hour with an X-ray source of Cu $K\alpha$ radiation (wavelength = 1.5406 \AA). The single-phase samples along with sample K:Nb-2.5-150 were imaged using scanning electron microscopy (SEM). A Zeiss Ultra 55 Field emission electron gun (FEG) SEM with a resolution of 100 nm was used to capture these SEM images. The electrons were accelerated with a 2-5 kV acceleration voltage. Due to the non-conducting nature of the samples they were coated with a layer of carbon via

Table 3.3: The parameters of the controlled [Nb] experiments. The temperature and KOH concentration is shown in the "experiment name" column, where the name of the experiment details this as follows: (experiment name)-[KOH]-temperature. The weight of niobium added to all the experiments was 0.5000(6) g. The shaded rows separate the different KOH concentrations.

Experiment name "Exp-[KOH]-T"	Volume KOH [mL]	[Nb] [$\frac{mol}{L}$]	K:Nb molar ratio
[Nb]-10-150	5	0.752	13.3
[Nb]-10-165	5	0.752	13.3
[Nb]-10-180	5	0.752	13.3
[Nb]-10-200	5	0.752	13.3
[Nb]-10-240	5	0.752	13.3
[Nb]-7.5-150	5	0.752	9.97
[Nb]-7.5-165	5	0.752	9.97
[Nb]-7.5-180	5	0.752	9.97
[Nb]-7.5-200	5	0.752	9.97
[Nb]-7.5-240	5	0.752	9.97
[Nb]-5-150	5	0.752	6.65
[Nb]-5-165	5	0.752	6.65
[Nb]-5-180	5	0.752	6.65
[Nb]-5-200	5	0.752	6.65
[Nb]-5-240	5	0.752	6.65

Table 3.4: The parameters of the controlled Na experiments. The temperature and NaOH concentration is shown in the "experiment name" column, where the name of the experiment details this as follows: (experiment name)-[NaOH]-temperature. The weight of niobium added to all the experiments was 0.5000(6) g. The shaded rows separate the different NaOH concentrations.

Experiment name "Exp-[NaOH]-T"	Volume NaOH [mL]	[Nb] [$\frac{mol}{L}$]	Na:Nb molar ratio
Na-10-150	1	3.76	2.66
Na-10-200	1	3.76	2.66
Na-10-240	1	3.76	2.66
Na-7.5-150	1	3.76	1.99
Na-7.5-200	1	3.76	1.99
Na-7.5-240	1	3.76	1.99

physical vapor deposition before imaging. Carbon graphite rods were heated in a vacuum to high temperatures using a 5 kV voltage source, evaporating the graphite depositing it on the samples.

4 Results

After synthesis the products were analyzed using X-ray diffraction and TOPAS [44,45] software to identify the phases and gather information about the phase purity, lattice parameters, strain and other factors. The local structures of the single-phase materials were investigated using Raman spectroscopy, and the morphology was studied using SEM.

4.1 Potassium Niobium Oxides XRD Analysis

A selection of the XRD patterns of the single-phase potassium niobate materials are shown in figure 4.1. The diffractogram patterns of the different potassium niobates show the variety of potassium niobate phases and structures which can be produced using hydrothermal synthesis. Some diffractogram did not show single-phase potassium niobates, although a dominant phase was present. $\text{K}_7\text{HfNb}_6\text{O}_{19} \cdot 10\text{H}_2\text{O}$ was the most common phase and many samples included 5-15 wt% $\text{K}_7\text{HfNb}_6\text{O}_{19} \cdot 13\text{H}_2\text{O}$ which was a common secondary phase.

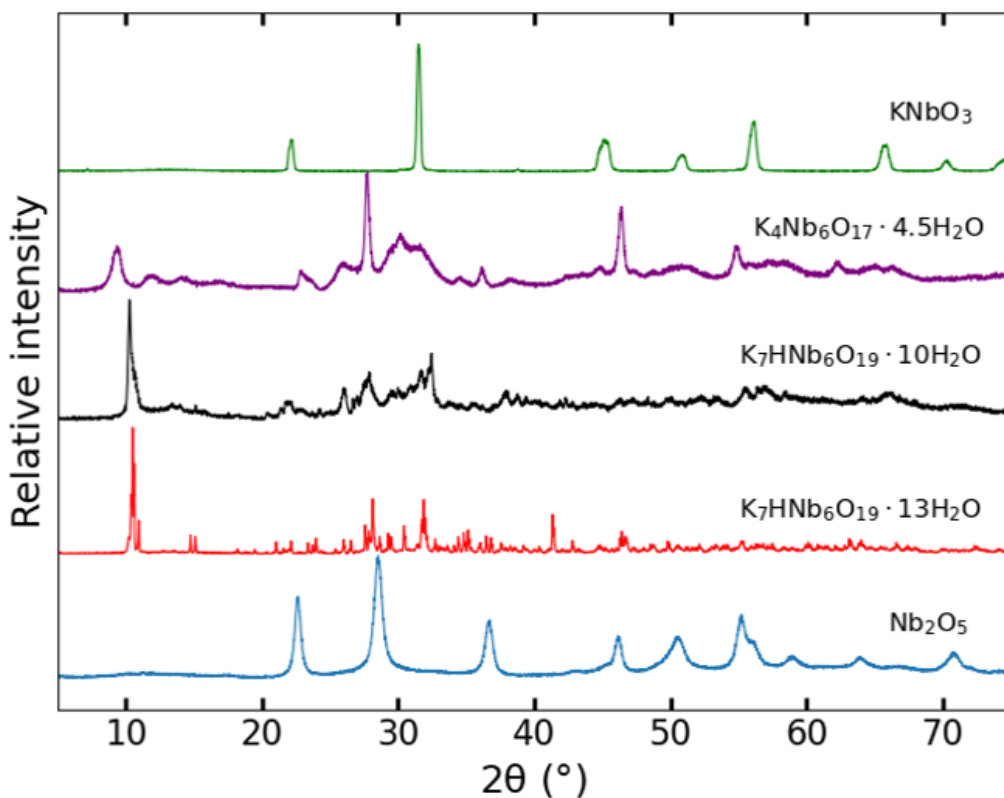


Figure 4.1: X-ray diffractograms of the four main potassium niobate phases synthesized, as well as the precursor T- Nb_2O_5 . The diffractograms are of single-phase materials, all the peaks in the diffractogram belong to the respective compound.

The diffractogram of the $\text{K}_7\text{HfNb}_6\text{O}_{19} \cdot 10\text{H}_2\text{O}$ and $\text{K}_4\text{Nb}_6\text{O}_{17}$ phases have low signal to noise ratio. $\text{K}_7\text{HfNb}_6\text{O}_{19} \cdot 13\text{H}_2\text{O}$ and $10\text{H}_2\text{O}$ are monoclinic phases with several small diffraction lines across the diffractogram. $\text{K}_7\text{HfNb}_6\text{O}_{19} \cdot 10\text{H}_2\text{O}$ has its

main peak at $10.2^\circ 2\theta$ while the $\text{K}_7\text{HNb}_6\text{O}_{19} \cdot 13\text{H}_2\text{O}$ has the main peak at $10.5^\circ 2\theta$. The $\text{K}_4\text{Nb}_6\text{O}_{17}$ phase has different degrees of hydration, between no hydration and 4.5 crystal water. The diffractogram for $\text{K}_4\text{Nb}_6\text{O}_{17}$ has some broad and weak diffraction lines throughout, with some more intense diffraction lines at for example 26 and $46^\circ 2\theta$. KNbO_3 is orthorhombic and has fewer diffraction lines with higher intensity than the other phases. Nb_2O_5 has broader peaks than most other phases due to the small crystallite size of ~ 18 nm as calculated using Rietveld refinement.

Table 4.1: Average lattice parameters of selected potassium niobate phases, along with crystallite size and β angle. Rietveld refinement of the diffraction patterns of $\text{K}_2\text{Nb}_2\text{O}_6 \cdot \text{H}_2\text{O}$ and $\text{K}_4\text{Nb}_6\text{O}_{17}$ was not done.

Phase	a [\AA]	b [\AA]	c [\AA]	β [$^\circ$]	Crystallite size [nm]
$\text{K}_7\text{HNb}_6\text{O}_{19} \cdot 10\text{H}_2\text{O}$	17.29 (± 0.03)	10.12 (± 0.03)	35.22 (± 0.05)	103.8 (± 0.1)	35-75
$\text{K}_7\text{HNb}_6\text{O}_{19} \cdot 13\text{H}_2\text{O}$	10.35 (± 0.02)	16.19 (± 0.01)	12.02 (± 0.02)	124.59 (± 0.02)	200+
$\text{K}_2\text{Nb}_2\text{O}_6 \cdot \text{H}_2\text{O}$	16	5	16	114	-
$\text{K}_4\text{Nb}_6\text{O}_{17}$	33.12	6.48	7.816	90	1 μm nanoplate

Table 4.1 shows the lattice parameters of the different potassium niobate phases, along with the β angle and crystallite size. KNbO_3 is not included in this table, the lattice parameters and the crystallite size are presented in section 4.3.1. The lattice parameters for $\text{K}_7\text{HNb}_6\text{O}_{19} \cdot 13\text{H}_2\text{O}$ and $\text{K}_7\text{HNb}_6\text{O}_{19} \cdot 10\text{H}_2\text{O}$ varied as a function of the temperature and KOH concentration and are shown as an average with the range in parenthesis next to it. The diffractogram patterns of $\text{K}_2\text{Nb}_2\text{O}_6 \cdot \text{H}_2\text{O}$ and $\text{K}_4\text{Nb}_6\text{O}_{17}$ were not Rietveld refined. $\text{K}_2\text{Nb}_2\text{O}_6 \cdot \text{H}_2\text{O}$ is not well studied in literature due to it being metastable and hard to produce, therefore the values given in this table are very approximate and are based on limited literature studies [17, 46]. $\text{K}_4\text{Nb}_6\text{O}_{17}$ has a morphology that makes the refinement inaccurate, so the literature values are given without refinement.

4.1.1 Phase Analysis from the Controlled K:Nb Molar Ratio

The phase composition data gathered from the XRD patterns of the controlled K:Nb molar ratio experiments are presented in figure 4.2. The stability diagram shows different synthesis conditions, the main ones being pH and temperature, lead to different phases being stable. At the lowest temperature and pH the Nb_2O_5 did not dissolve. Increasing the temperature while keeping pH low lead to the formation of $\text{K}_4\text{Nb}_6\text{O}_{17}$. Increasing pH while keeping temperature low lead to the

formation of $K_7HNb_6O_{19} \cdot 13H_2O$ at moderate pH and $K_7HNb_6O_{19} \cdot 10H_2O$ at high pH. Increasing both pH and temperature caused the formation of orthorhombic $KNbO_3$, the temperature needed to be above 7.5 M for all experiments.

An interesting observation is that the three samples produced at 5 M KOH were totally dissolved, the product of the synthesis was a clear solution. The phases were precipitated in ethanol before filtering and characterization. The rest of the products were precipitated in the autoclave without ethanol. The $KNbO_3$ samples were not completely white powders, instead containing a lime-green hue. This lime green hue was present for all the $KNbO_3$ samples except K:Nb-10-200.

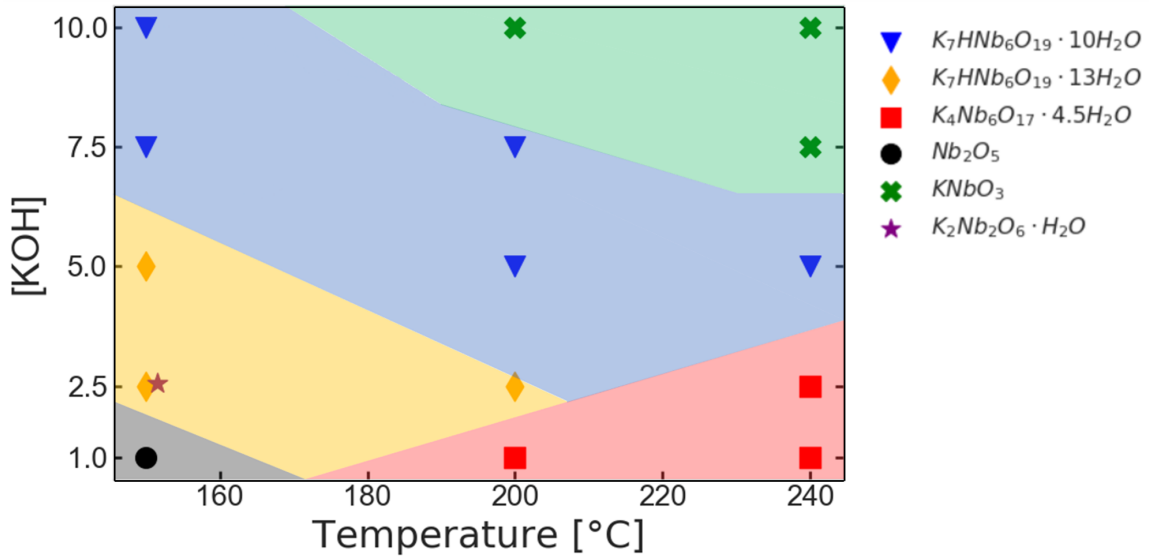


Figure 4.2: Stability diagram of potassium niobates as a function of temperature and KOH concentration with controlled K:Nb ratio. Sample K:Nb-2.5-150 was identified using the Raman spectra which has some uncertainties related to the identity of the phases. The stability areas and borders are approximate because of limited data.

Note that the sample made at 150 °C and 2.5 M KOH is identified as $K_7HNb_6O_{19} \cdot 13H_2O$ by the Raman spectrum, shown in figure 4.9. This sample came out of the autoclave with no liquid, only a wet crystallized product. All the liquid was seemingly absorbed into one large and hard crystallized clump, no evidence of an autoclave leak was found. The X-ray diffractogram was not identifiable using the monoclinic $K_7HNb_6O_{19} \cdot 13H_2O$ with the P21 space group, as will be discussed further in section 5.2.1.

4.1.2 Phase Analysis from the Constant Niobium Concentration Experiments

Figure 4.3 shows the stability of phases at different temperature and pH for the samples made with constant niobium concentration as described in table 3.3. The stability diagram shows that $K_7HNb_6O_{19} \cdot 10H_2O$ is the most stable phase at low temperature and pH below 7.5 M, $K_7HNb_6O_{19} \cdot 13H_2O$ only produced at the highest temperature at 5 M KOH. At 165 °C and high pH $KNbO_3$ was the stable

phase. The KNbO_3 had two different crystal structures, monoclinic and orthorhombic. The monoclinic KNbO_3 is metastable and was only synthesized at temperatures below 240 °C. The synthesis parameters for the constant niobium concentration experiments are described in table 3.3.

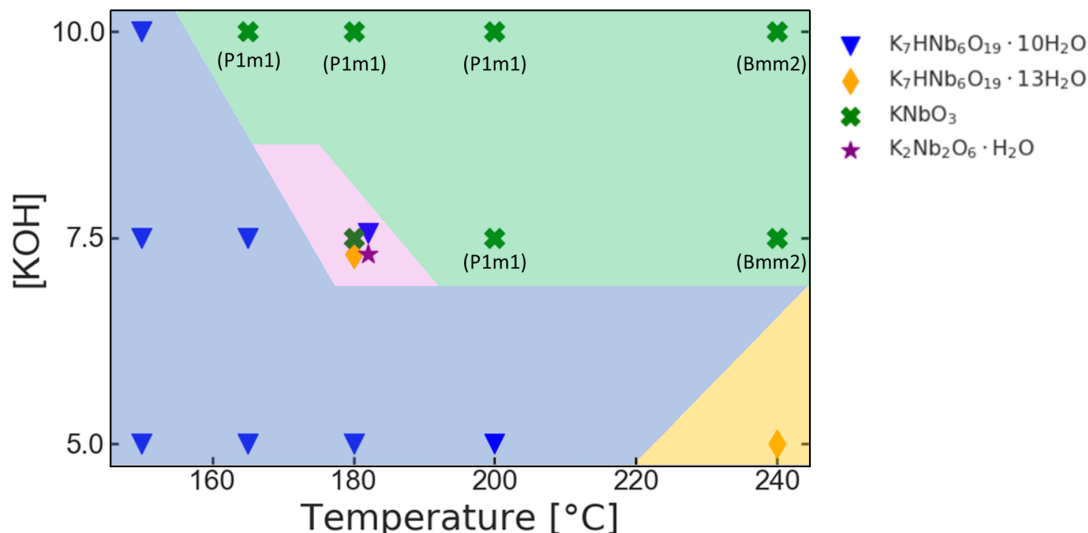


Figure 4.3: Stability diagram of potassium niobates as a function of temperature and KOH concentration with constant niobium concentration. The pink area represents an area on the border between two phases ($\text{K}_7\text{HNB}_6\text{O}_{19} \cdot 10\text{H}_2\text{O}$ and KNbO_3) where the product contained intermediate phases. The space group of the different crystal structures is noted, P1m1 for the monoclinic KNbO_3 and Bmm2 for the orthorhombic KNbO_3 . The stability areas and borders are approximate because of limited data.

The pink area of figure 4.3 shows a border region that had several phases at the same time. In addition to the four alkali niobate phases that were found, the XRD pattern had diffraction lines that were not identified. There was some solid product in the autoclave which had a lime green hue (KNbO_3) and the hexaniobate phases precipitated from the free niobates in solution when the products were washed in ethanol. Two of the samples made with 5 M KOH contained little to no solids, [Nb]-5-180 was a totally clear solution and [Nb]-5-240 was a milky white suspension with little to no precipitate at the bottom. The rest of the samples contained solid product and were washed and filtered in ethanol before drying and analysis. As with the K:Nb molar ratio samples the KNbO_3 samples were not white powders, instead the product had a lime-green shine. This lime green hue was present for all the KNbO_3 samples, and seemed to be stronger and brighter for samples made with high KOH concentration.

4.2 Sodium Niobium Oxides

The reaction kinetics for the reaction between niobium oxide and sodium hydroxide is fast, even at low temperature and NaOH concentration the stable sodium niobates were $\text{Na}_2\text{Nb}_2\text{O}_6 \cdot \text{H}_2\text{O}$ and NaNbO_3 . The XRD pattern shown in figure 4.4 gives information about phase and structure of the sodium niobates. The

sample made at 150 °C using 10 M NaOH had very small crystallite size as seen in figure 4.11. The synthesis conditions for the sodium niobate phases are presented in table 3.3.

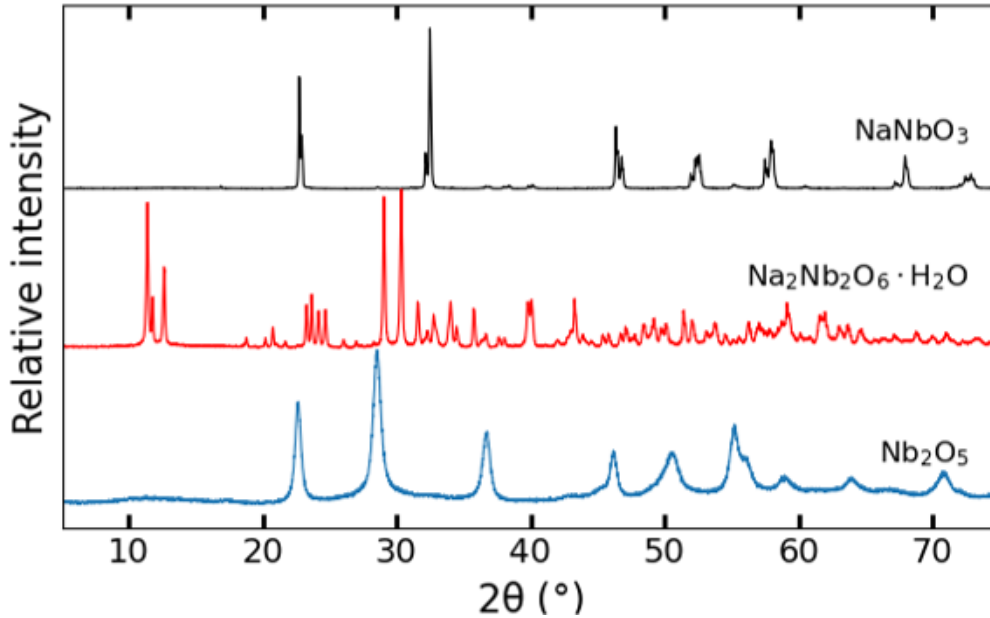


Figure 4.4: X-ray diffractogram of the two main sodium niobate phases synthesized, as well as the precursor Nb₂O₅. Na₂Nb₂O₆ · H₂O is a highly crystalline material with a monoclinic crystal structure, which means the diffractogram has many diffraction lines. NaNbO₃ has orthorhombic crystal structure and has fewer sharp and intense diffraction lines.

Figure 4.5 shows the stability diagram of sodium niobium oxides and is based on the XRD patterns of the sodium niobates. Using sodium hydroxide gives faster reaction kinetics compared to potassium hydroxide. NaNbO₃ forms at even lower temperatures, only at 150 °C and 7.5 M NaOH does Na₂Nb₂O₆ · H₂O form. This phase is a precursor to NaNbO₃ [29], and reacts at sufficiently high temperatures and NaOH concentration. This phase had lattice parameters almost identical to the literature values of $a=17.05$, $b=5.03$, $c=16.49$ and $\beta=114.0^\circ$. The crystallite size was 89 nm according to the Rietveld refinement, but due to the fiber morphology of this phase the average crystallite size is not well represented by this value.

4.3 Structure of Potassium Niobates

4.3.1 Lattice Parameters of KNbO₃

For each sample the crystallite size and lattice parameters were calculated using Rietveld analysis. Rietveld analysis can not calculate crystallite size higher than ~200 nm, above this crystallite size other methods such as SEM must be used to determine particle and crystallite size accurately. The structural analysis was done with a focus on lattice parameters, crystallite size, lattice strain, atomic positions, thermal strain and occupancy. The KNbO₃ from sample [Nb]-7.5-180 was hard

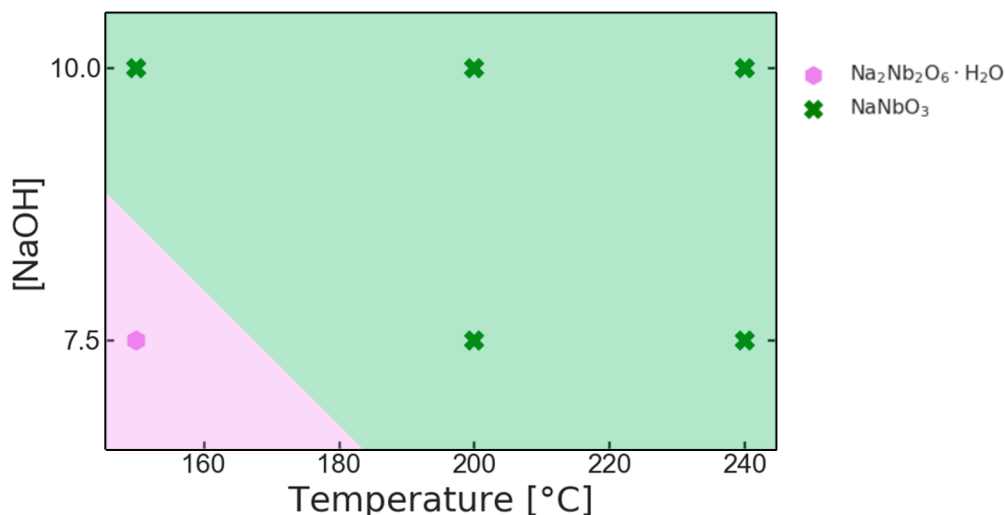


Figure 4.5: Stability diagram of sodium niobates as a function of temperature and NaOH concentration. Only at the lowest temperature and pH did $\text{Na}_2\text{Nb}_2\text{O}_6 \cdot \text{H}_2\text{O}$ form, showing fast reaction kinetics for the sodium niobates. The stability areas and borders are approximate because of limited data.

to analyze due to the multi-phase nature of the sample and its XRD spectrum of overlapping peaks.

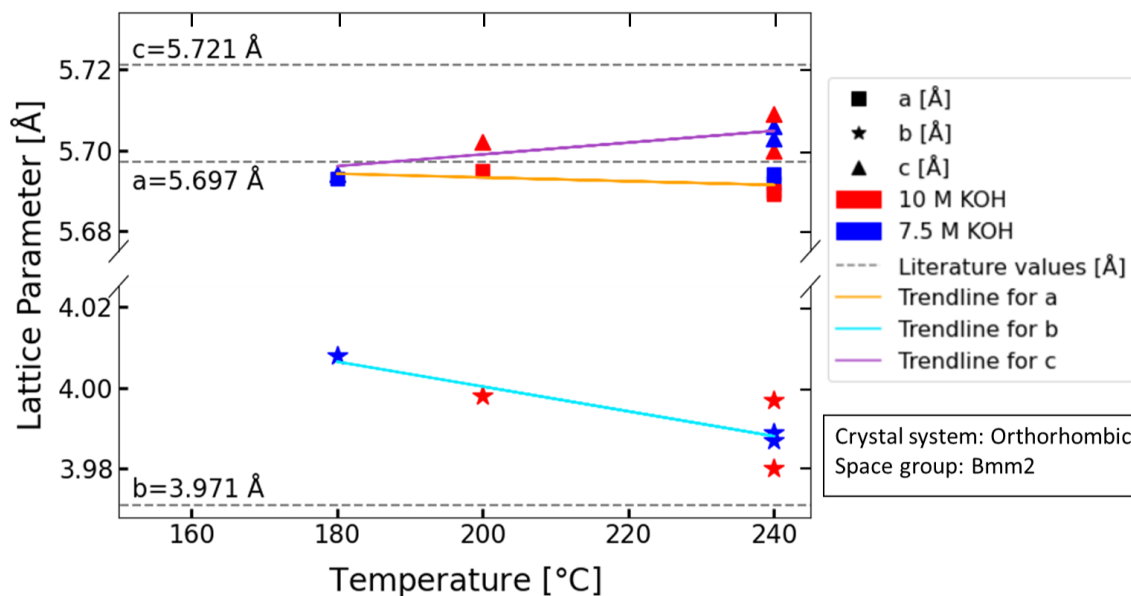


Figure 4.6: Lattice parameters of orthorhombic KNbO_3 for 10 M (red) and 7.5 M (blue) KOH. The dashed gray horizontal lines represent the literature values of the lattice parameters (from PDF database, PDF:00-032-0822 [47]).

Lattice parameters of orthorhombic KNbO_3 are shown in figure 4.6. Orthorhombic KNbO_3 was the stable phase between 180 degrees and 240 °C and at high potassium concentration, 7.5 M (blue) and 10 M (red) KOH. At the lowest temperatures the lattice parameters a and c are similar and the b parameter is

higher than the literature value. At higher temperatures the b and c lattice constants approach the literature values, a increases while b decreases. The c parameter does not change in a significant way with temperature, pH has no apparent effect on lattice parameters.

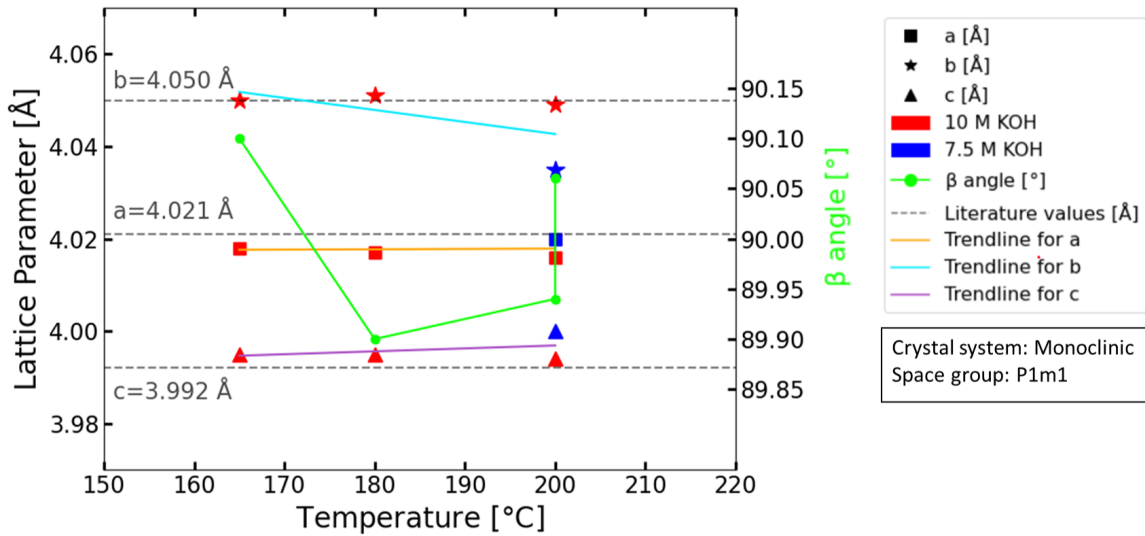


Figure 4.7: Lattice parameters of monoclinic KNbO_3 for 10 M (red) and 7.5 M (blue) KOH, as well as the β angle (green). The dashed gray horizontal lines represent the literature values of the lattice parameters (from [40]).

The lattice parameters of monoclinic KNbO_3 , shown in figure 4.7, has low variability of the lattice parameters with temperature, but alkalinity has an apparent effect. For the 10 M KOH experiments the lattice parameters of the monoclinic KNbO_3 remain close to the literature values across the entire temperature range, but for 7.5 M KOH the b and c parameter are closer to the a parameter. The β angle varied between 90.10 and 89.90° with the angle approaching 90° at higher temperatures.

The crystallite size was calculated for all the KNbO_3 samples, both monoclinic and orthorhombic. The monoclinic samples reached crystallite size above 200 nm at all temperatures, meaning exact value unknown as Rietveld refinement cannot calculate crystallite size above ~ 200 nm. The orthorhombic sample at 180 °C and 7.5 M KOH had the smallest crystallite size which increased with temperature. At 240 °C the samples had a range of crystallite sizes between 67 and 155 nm. The two lowest crystallite sizes at 240 °C were from the K:Nb experiments and the largest were from the [Nb] experiments.

4.3.2 Local Structure of Potassium Niobates

The local structure of the potassium niobates were studied using Raman spectroscopy. The single-phase potassium niobates were investigated to determine chemical bonds and vibrational modes within the different compounds and the Raman spectrum shown in figure 4.9 was used to identify sample K:Nb-2.5-150

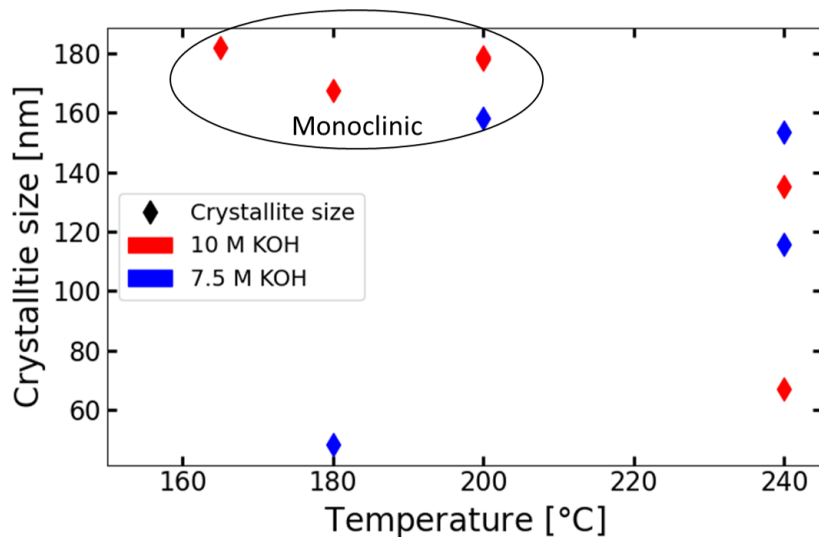


Figure 4.8: Crystallite size of KNbO_3 , both monoclinic (within the circle) and orthorhombic, as a function of temperature and KOH concentration. The crystallite size was calculated using Rietveld refinement. Rietveld analysis can not accurately calculate crystallite size above ~ 200 nm, meaning the monoclinic KNbO_3 samples had above 200 nm sized crystallites. The orthorhombic samples at 240 °C are from both the [Nb] and K:Nb experiments, the K:Nb experiments have the two smallest crystallite sizes while the [Nb] experiments have the two largest.

which could not be identified by XRD.

The bands of the Raman spectra are marked in figure 4.9, the vibrational modes represented by the bands are presented in table 4.2. When comparing the Raman spectra of different potassium niobates the spectra can be divided into three main areas. In general the bands below 300 cm^{-1} represent internal vibrational modes, libration modes, and the longest Nb-O bending modes. Bands between 300 and 700 cm^{-1} belong to the medium length Nb-O bonds, such as the edge shared octahedra Nb-O stretching mode. The bands at the highest wavenumbers above 700 cm^{-1} belong to the shortest Nb-O stretching modes, especially the $\text{Nb}=\text{O}_t$ double bonds. monoclinic and orthorhombic KNbO_3 have nearly identical Raman spectra, as is expected when the difference in local structure is small as seen in figure 2.7. The three hexaniobate samples, $\text{K}_7\text{HfNb}_6\text{O}_{19} \cdot 10 \text{ H}_2\text{O}$, $\text{K}_7\text{HfNb}_6\text{O}_{19} \cdot 13 \text{ H}_2\text{O}$ and $\text{K}_4\text{Nb}_6\text{O}_{17}$, have similar bands because of some similarities in local structure of the hexaniobate anions. The bands they share are at 225, 290, 530, 840 and 890 cm^{-1} . $\text{K}_4\text{Nb}_6\text{O}_{17}$ has a shift in wavenumber for the band at 840 compared to the other potassium niobate samples, up to about 860 cm^{-1} .

Sample K:Nb-2.5-150 is identified as $\text{K}_7\text{HfNb}_6\text{O}_{19} \cdot 13 \text{ H}_2\text{O}$ & $\text{K}_2\text{Nb}_2\text{O}_6 \cdot \text{H}_2\text{O}$ based on the Raman spectrum, which is what this sample is marked as in figure 4.2, 4.9 and 4.13. The unit cell for $\text{K}_2\text{Nb}_2\text{O}_6 \cdot \text{H}_2\text{O}$ is similar to $\text{Na}_2\text{Nb}_2\text{O}_6 \cdot \text{H}_2\text{O}$. The local structure appears to be similar as well although this phase is not well studied [17]. The Raman spectrum of $\text{Na}_2\text{Nb}_2\text{O}_6 \cdot \text{H}_2\text{O}$ has high intensity bands at 220 and 880 cm^{-1} , which is very similar to $\text{K}_2\text{Nb}_2\text{O}_6 \cdot \text{H}_2\text{O}$ [48]. Because these bands

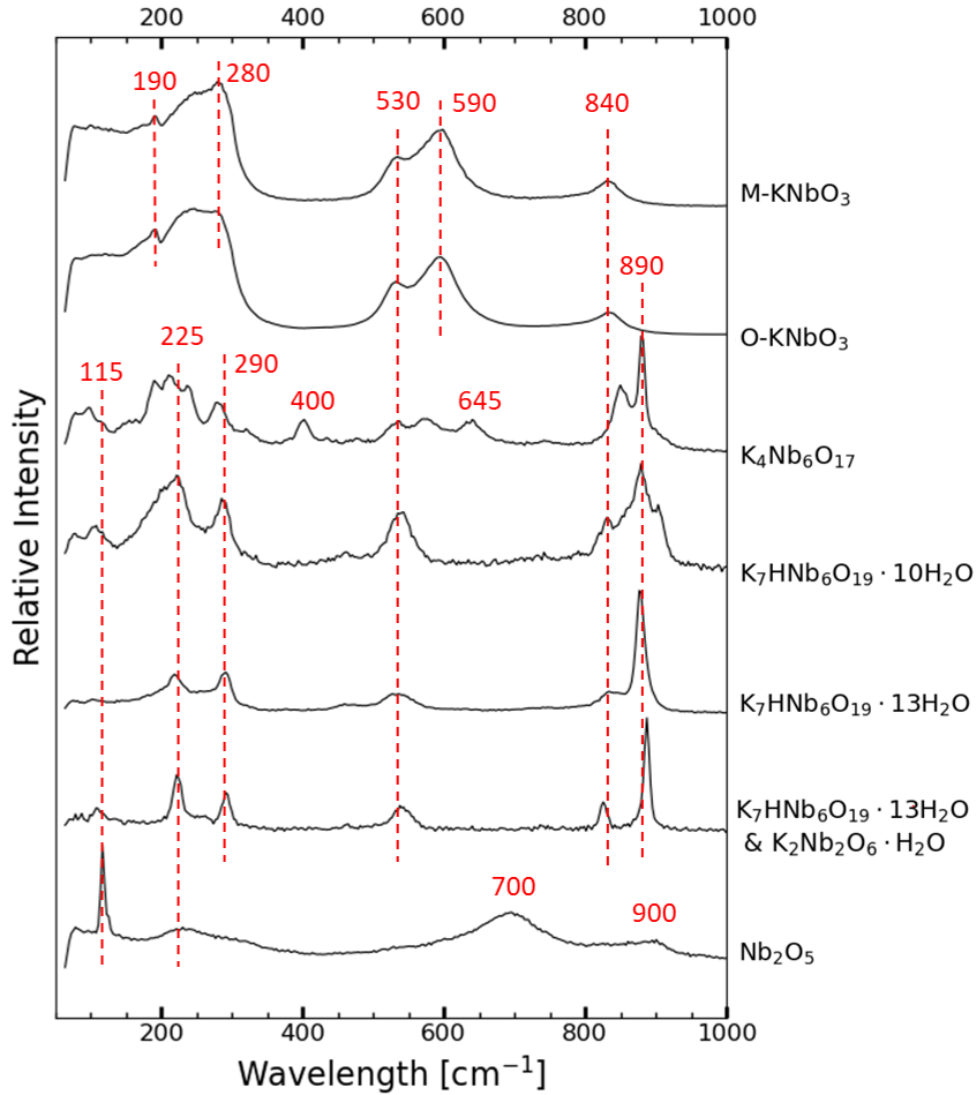


Figure 4.9: Raman spectra of each single-phase potassium niobate material as well as the precursor Nb_2O_5 . The wavenumbers of the different bands are marked in red. The spectrum marked $\text{K}_7\text{HNB}_6\text{O}_{19} \cdot 13\text{H}_2\text{O}$ & $\text{K}_2\text{Nb}_2\text{O}_6 \cdot \text{H}_2\text{O}$ is the Raman spectrum for sample K:Nb-2.5-150 and has uncertainty related to phase composition.

overlap with the bands for $\text{K}_7\text{HNB}_6\text{O}_{19} \cdot 13\text{H}_2\text{O}$ they are not easy to distinguish.

In table 4.2 the different oxygen atoms are referred to by their position in the octahedra. O_t refers to the terminal oxygen connected to the Nb by a double bond, O_b refers to the bridging oxygen, which connects two niobium atoms on the outside of the octahedra and O_c refers to the oxygen in the center of a cluster of six octahedra. The $\text{K}_2\text{Nb}_2\text{O}_6 \cdot \text{H}_2\text{O}$ is not a single phase material. Therefore the bands that might belong to pyrochlore $\text{K}_2\text{Nb}_2\text{O}_6$ or $\text{K}_2\text{Nb}_2\text{O}_6 \cdot \text{H}_2\text{O}$ fibers are not included in the table. The bands for $\text{K}_2\text{Nb}_2\text{O}_6 \cdot \text{H}_2\text{O}$ is similar to $\text{Na}_2\text{Nb}_2\text{O}_6 \cdot \text{H}_2\text{O}$.

Table 4.2: Table of the vibrational modes representing the bands found in the potassium samples, as reported by literature [17, 48–60].

Compound	Wavenumber [cm^{-1}]	Vibrational Mode
KNbO ₃	190	Nb-O-Nb A ₁ (TO) & A ₁ (LO)
	280	Nb-O-Nb A ₁ (TO) & A ₁ (LO)
	530	B ₁ (TO)
	590	A ₁ (TO)
	840	Nb=O _t surface groups
K ₄ Nb ₆ O ₁₇ · xH ₂ O	80-120	K and Nb translations
	190-480	Nb-O _b -Nb bending mode and octahedra libration
	530-640	Long Nb-O bonds from symmetric and asymmetric NbO ₆ stretching vibrations
	860, 890	Nb=O _t stretching modes
K ₇ HNb ₆ O ₁₉ · 10 H ₂ O	80-120	Other molecular vibrations, external modes
	225	Nb-O _b -Nb bending modes
	290	Nb-O _c stretching mode
	530	Nb-O edge shared octahedra stretching mode
	840, 890	Nb=O _t stretching modes
K ₇ HNb ₆ O ₁₉ · 13 H ₂ O	225	Nb-O _b -Nb bending modes
	290	Nb-O _c stretching mode
	530	Nb-O edge shared octahedra stretching mode
	840, 890	Nb=O _t stretching mode
Nb ₂ O ₅	115	Librational modes of the NbO ₆ octahedra and NbO ₇ pentagonal dipyramids
	225	Wide band from variable length Nb-O _b -Nb bending modes
	700	Low distortion niobium oxide octahedra
	900	Nb=O _t surface groups

4.4 Structure of Sodium Niobates

4.4.1 Lattice Parameters of NaNbO_3

The lattice parameters and crystallite size of the sodium niobates were calculated using Rietveld refinement. As with the orthorhombic KNbO_3 the lattice parameters a and c are the same at low temperatures, but diverge at higher temperatures. All lattice parameters approach the literature values at higher temperatures as expected. NaOH concentration does not seem to affect the lattice parameters, temperature is the parameter that affects the lattice constants in a significant way.

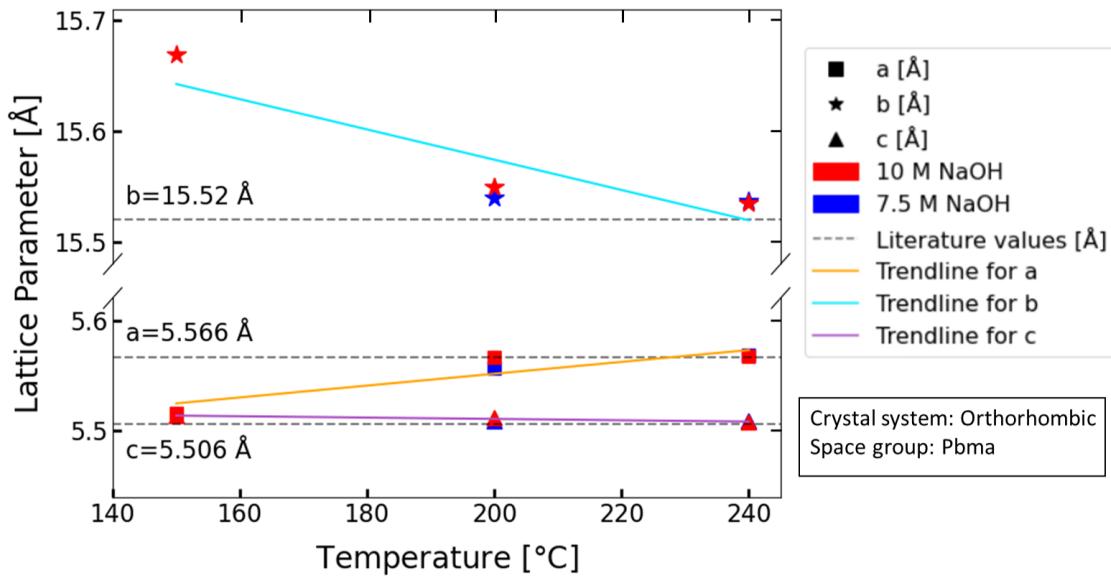


Figure 4.10: Lattice parameters of NaNbO_3 for 10 M (red) and 7.5 M (blue). The dashed gray horizontal lines represent the literature values of the lattice parameters (from PDF database, PDF:00-032-0822 [47]).

The crystallite size is small for the sample made at 150 °C but with higher temperature the crystallite size quickly reached above ~ 200 nm. The samples Na-10-150 and Na-10-200 have crystallite sizes below 200nm, the other samples have crystallite sizes at or above ~ 200 nm which means the values shown in figure 4.11 are not accurate. Other methods such as SEM are needed to accurately assess the crystallite and particle size of these samples. It seems higher temperature and lower NaOH concentration leads to higher crystallite size, though the samples with above ~ 200 nm are hard to compare because the exact size is unknown.

4.4.2 Local Structure of Sodium Niobates

The local sodium niobate structure was studied using Raman spectroscopy and is shown in figure 4.12. The different Nb-O bond lengths and vibrational modes in NaNbO_3 and $\text{Na}_2\text{Nb}_2\text{O}_6 \cdot \text{H}_2\text{O}$ is represented by bands which are marked in figure 4.12 and assigned a vibrational mode in table 4.3. NaNbO_3 has several bands in the $50\text{-}300\text{ cm}^{-1}$ region, due to the tilted NbO_6 octahedra in the structure. These

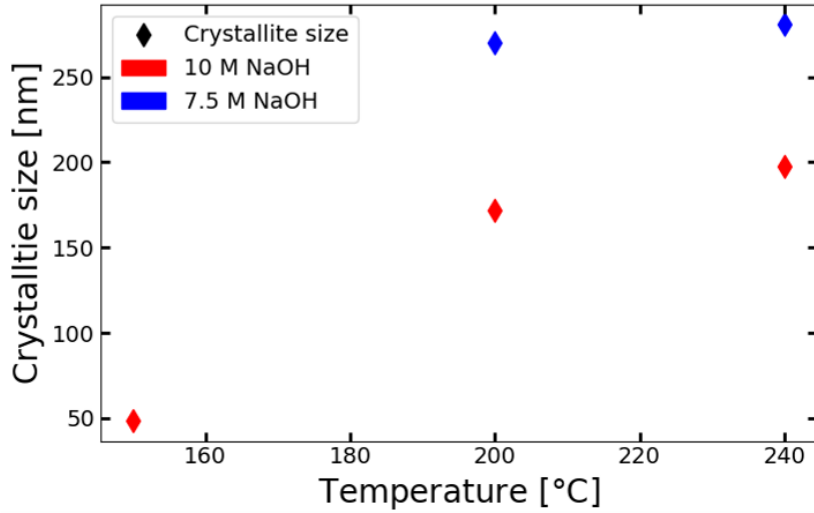


Figure 4.11: Crystallite size of NaNbO_3 as a function of temperature and NaOH concentration. The crystallite size was calculated using Rietveld refinement.

bands are from the triply degenerate $\nu_6(\text{F}_{2u})$ and $\nu_5(\text{F}_{2g})$ modes which have split due to the tilted octahedra, as well as tilted octahedra librational modes [48]. The bands for NaNbO_3 between 500 and 600 cm^{-1} belong to the Nb-O-Nb bond between the corner shared octahedra. $\text{Na}_2\text{Nb}_2\text{O}_6 \cdot \text{H}_2\text{O}$ has two main bands that are more intense than the others at 220 and 880 cm^{-1} . These bands represent the Nb-O-Nb bending mode at 220 cm^{-1} and the Nb=O_t stretching mode at 880 cm^{-1} .

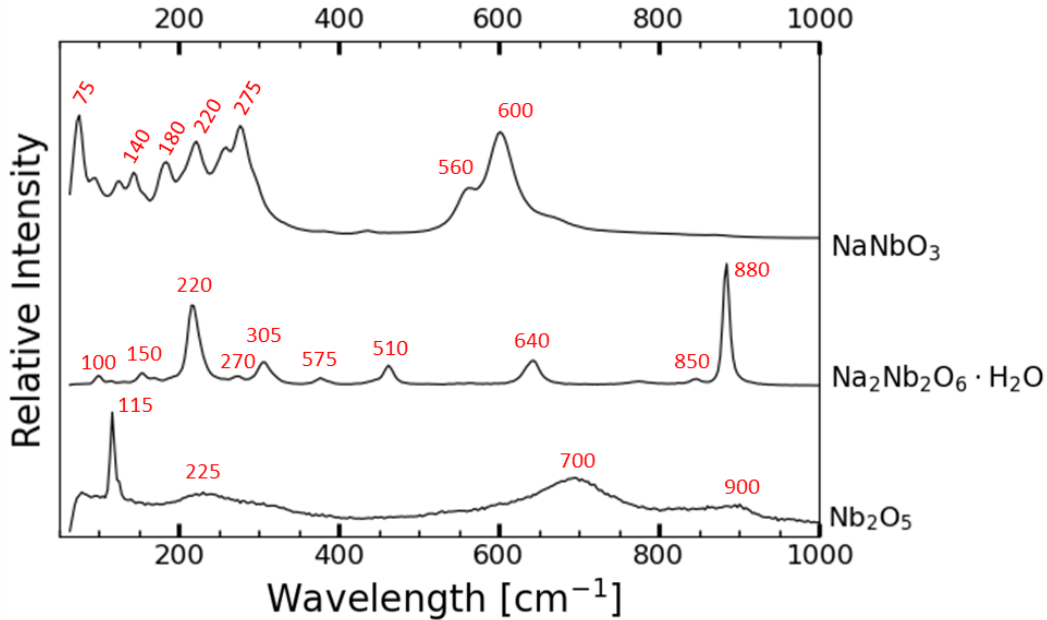


Figure 4.12: Raman spectroscopy of both sodium niobate materials as well as the precursor Nb_2O_5 . The wavenumbers of the different bands are marked in red.

Table 4.3: Table of the vibrational modes representing the bands observed in the spectra of sodium niobate samples and as reported by literature [48, 50–61]. O_t refers to the terminal oxygen connected to the Nb by a double bond, O_b refers to the bridging oxygen, which connects two niobium atoms on the outside of the octahedra and O_c refers to the oxygen in the center of a cluster of octahedra.

Compound	Wavenumber [cm^{-1}]	Vibrational Mode
NaNbO ₃	150-275	Nb-O-Nb stretching mode Belongs to triply degenerate $\nu_6(F_{2u})$ and $\nu_5(F_{2g})$ modes Split due to tilted octahedra
	560	B ₁ (TO)
	600	A ₁ (TO)
Na ₂ Nb ₂ O ₆ · H ₂ O	220	Nb-O-Nb T _{2g} bending mode
	270, 305	Long NbO bonds A _{1g} breathing vibration
	460	Nb-O _b -Nb bending mode
	530-640	Nb-O-Nb stretching mode
	850, 890	Nb=O _t stretching mode
Nb ₂ O ₅	115	Librational modes of the NbO ₆ octahedra and NbO ₇ pentagonal dipiramids
	225	Wide band from variable length Nb-O _b -Nb bending mode
	700	Low distortion niobium oxide octahedra
	900	Nb=O _t surface groups

4.5 Morphology of Alkali Niobates

SEM images of the single-phase alkali niobates, one for each single-phase material, as well as a multi-phase material such as K:Nb-2.5-150 are presented in figure 4.13. The potassium niobates show agglomeration in all the different materials. The monoclinic KNbO_3 , shown in figure 4.13f) has rectangular prism morphology where the rectangular prisms are agglomerated together. The fibrous crystals in figure 4.13c) are $\text{K}_2\text{Nb}_2\text{O}_6 \cdot \text{H}_2\text{O}$ which seem to stick out of agglomerated $\text{K}_7\text{HNb}_6\text{O}_{19} \cdot 13\text{H}_2\text{O}$ crystals, appearing to grow from them. $\text{K}_4\text{Nb}_6\text{O}_{17}$, shown in figure 4.13d), have thin nanoplate morphology where the plates look like rose petals folded around each other. These three materials have a uniform morphology, the other materials are agglomerated into irregularly shaped clumps. The samples were not well dispersed before SEM imaging because some phases can change structure or be dissolved if dispersed in a solvent such as ethanol or water.

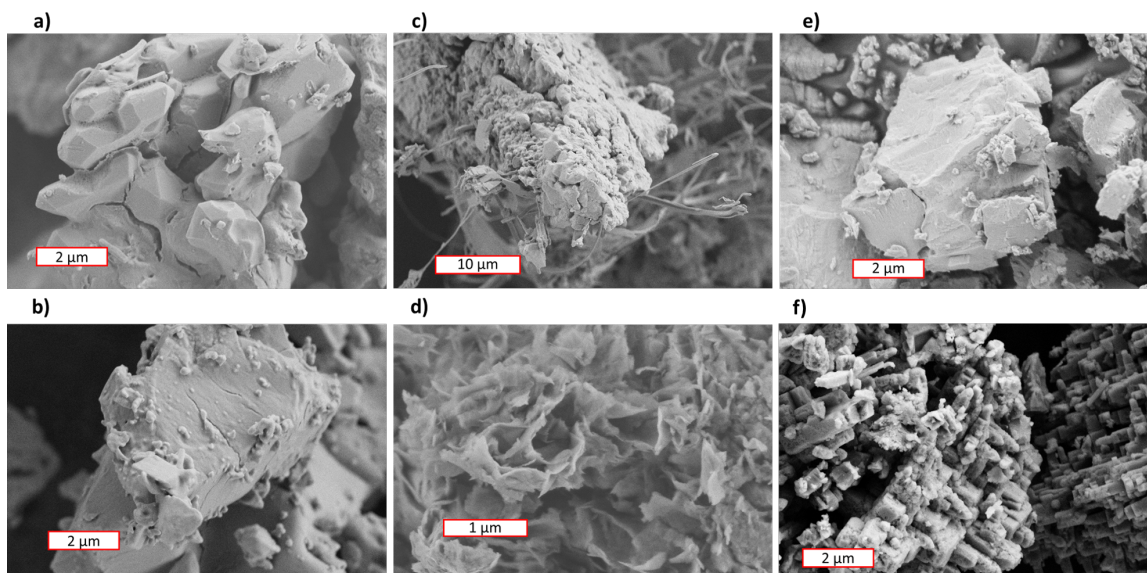


Figure 4.13: SEM images of the potassium niobate compounds a) $\text{K}_7\text{HNb}_6\text{O}_{19} \cdot 10\text{H}_2\text{O}$, b) $\text{K}_7\text{HNb}_6\text{O}_{19} \cdot 13\text{H}_2\text{O}$, f) mixed phase comprised of $\text{K}_7\text{HNb}_6\text{O}_{19} \cdot 13\text{H}_2\text{O}$ & fibers of $\text{K}_2\text{Nb}_2\text{O}_6 \cdot \text{H}_2\text{O}$, d) $\text{K}_4\text{Nb}_6\text{O}_{17}$, e) orthorhombic KNbO_3 and f) monoclinic KNbO_3 . The agglomerated phase in c) is not securely identified, but the evidence has suggested $\text{K}_7\text{HNb}_6\text{O}_{19} \cdot 13\text{H}_2\text{O}$ or pyrochlore $\text{K}_2\text{Nb}_2\text{O}_6$.

The SEM images of the presented sodium niobates, shown in figure 4.14, show uniform morphology; Rectangular prism morphology for NaNbO_3 shown in figure 4.14a) and fibrous morphology for the $\text{Na}_2\text{Nb}_2\text{O}_6 \cdot \text{H}_2\text{O}$ fibers shown in figure 4.14c). The $\text{Na}_2\text{Nb}_2\text{O}_6 \cdot \text{H}_2\text{O}$ fibers in figure 4.14b) appear along with NaNbO_3 cubes, which have formed from the fibers as $\text{Na}_2\text{Nb}_2\text{O}_6 \cdot \text{H}_2\text{O}$ is a known precursor to NaNbO_3 . A close up image of the NaNbO_3 , shown in figure 4.14d), show rectangular prisms that have a size range between 100 nm and 1 μm .

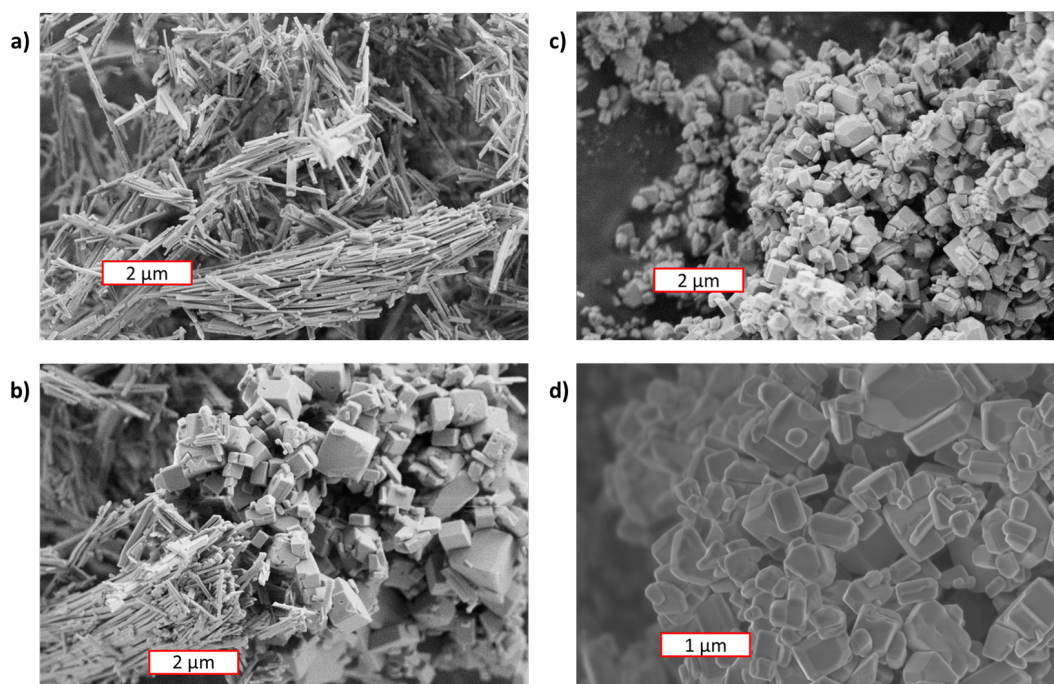


Figure 4.14: SEM images of the sodium niobate compounds **a)** $\text{Na}_2\text{Nb}_2\text{O}_6 \cdot \text{H}_2\text{O}$, **b)** $\text{K}_2\text{Nb}_2\text{O}_6 \cdot \text{H}_2\text{O}$ (fibers) NaNbO_3 (cubes), **c)** NaNbO_3 and **d)** NaNbO_3 imaged with an in-lens detector as opposed to the back scattered electrons used to capture the other images.

5 Discussion

5.1 Synthesis Conditions and Their Effects on Alkali Niobates

5.1.1 K:Nb Molar Ratio Versus Constant Niobium Concentration

The differences between the synthesis parameters of K:Nb molar ratio and [Nb] experiments had noticeable effects. Three main factors differentiate the synthesis conditions for controlled K:Nb molar ratio experiments compared to the constant niobium concentration experiments: total volume of KOH, K:Nb molar ratio and the niobium concentration. The constant niobium concentration experiments have higher volume, higher K:Nb ratio and lower niobium concentration. Which of these factors had the biggest effect is unknown, it is most likely a combination of all three. The differences in the results produced from the two different experiment series are summarized below.

- Monoclinic KNbO_3 was only produced with the constant [Nb] experiment synthesis conditions, K:Nb-10-200 gave orthorhombic KNbO_3 while [Nb]-10-200 gave monoclinic KNbO_3
- At 7.5 M and 200 °C, the constant [Nb] experiments produced KNbO_3 while controlled K:Nb ratio did not
- Crystallite sizes for KNbO_3 was higher for constant [Nb] experiments than for controlled K:Nb molar ratio experiments at 240 °C
- Solids precipitated at 5 M KOH in some of the [Nb] experiments but no precipitation for the K:Nb experiments at this concentration of KOH

These differences will be discussed one by one, how the synthesis conditions could affect the differences seen between the two experiment series. To study the effects of niobium concentration, K:Nb molar ratio and volume independently of pH and temperature the samples that were compared were produced at the same temperatures and pH. Samples that were compared were from the controlled K:Nb ratio and constant niobium concentration experiments with the same pH and temperature, which were samples produced at 5-10 M KOH and 150 °C, 200 °C and 240 °C.

The effects of higher K:Nb molar ratio on alkali niobate phases are numerous. Higher K:Nb molar ratio leads to increased driving force for reaction in equilibrium, as described by equation 3, leading to KNbO_3 forming at lower temperature. High K:Nb molar ratio changes solubility conditions which could help precipitate solids at 5 M KOH. Increased alkalinity, which goes hand in hand with an increased K:Nb molar ratio when moles of Nb_2O_5 is constant, increases kinetics. With high pH the Lindqvist anion breaks down into smaller NbO_6 octahedra clusters [17], which can then assemble into new alkali niobate structures. The stability of other intermediate phases could also change with changes in alkalinity. Some of these intermediate

phases decrease the energy barrier to form KNbO_3 and are most likely important steps in the formation mechanism of this phase, as will be discussed further. In the experiments with high K:Nb molar ratio KNbO_3 was synthesized at 7.5 M KOH and 200 °C, which did not happen for the low K:Nb molar ratio sample at this temperature. The samples with higher K:Nb molar ratio gave monoclinic KNbO_3 while the samples with low K:Nb ratio gave only orthorhombic KNbO_3 .

Niobium concentration had an effect on the reaction kinetics and driving forces, as well as the crystal structure of KNbO_3 . The K:Nb experiments had 3.76 M Nb and the [Nb] experiments at 0.75 M Nb. At 200 °C and 7.5 M KOH the products from the two different experiment series were not the same. When the concentration of niobium was high, $3.76 \frac{\text{mol}}{\text{L}}$, KNbO_3 did not form. When the concentration of niobium was low, $0.75 \frac{\text{mol}}{\text{L}}$, KNbO_3 formed. The experiments with lower niobium concentration lead to synthesis of monoclinic KNbO_3 , higher niobium concentration lead to the formation of orthorhombic KNbO_3 at all temperatures.

The volume of solution could have had an impact on precipitating samples at 5 M KOH. The autoclave from the controlled K:Nb molar ratio experiments which were made with 1 mL KOH solution contained no precipitate while the samples made with 5 mL solution had precipitated solids at 150 °C, 165 °C and 200 °C. Volume and fill factor varies greatly in the literature, and is seemingly not as important a factor as the K:Nb ratio and niobium concentration.

Considering these results, the factors that play an important role in formation of KNbO_3 is low niobium concentration and high K:Nb molar ratio. Which of these factors is most important is not possible to determine with this study alone. These synthesis parameters are not as important as temperature and alkalinity, but seem to have a noticeable effect on the phase formation.

5.1.2 Sodium Compared to Potassium on Reaction Kinetics

Sodium hydroxide as the precursor means faster kinetics compared to potassium hydroxide. At 150 °C and 7.5-10 M KOH the material that formed was $\text{K}_7\text{HfNb}_6\text{O}_{19} \cdot \text{H}_2\text{O}$. Using sodium hydroxide at the same temperature and alkalinity resulted in NaNbO_3 and $\text{Na}_2\text{Nb}_2\text{O}_6 \cdot \text{H}_2\text{O}$ forming. No $\text{Na}_7\text{HfNb}_6\text{O}_{19} \cdot 15\text{H}_2\text{O}$ formed, the temperature and NaOH concentration were too high. The time spent in the autoclave was kept at 18 hours, unchanged from the potassium niobates, which is longer than needed for the sodium niobate synthesis.

The sodium niobate phases have more uniform morphology compared to the potassium niobates. The sodium niobate phases had rectangular prism morphology for NaNbO_3 and fiber morphology for $\text{Na}_2\text{Nb}_2\text{O}_6 \cdot \text{H}_2\text{O}$ with low degree of agglomeration. Monoclinic KNbO_3 also had rectangular prism morphology with some agglomeration while orthorhombic KNbO_3 showed a high degree of agglomeration and had no regular morphology.

5.2 The Formation of Alkali Niobate Phases

5.2.1 Identifying a Low Temperature Low pH Potassium Niobate

To identify the potassium niobate made with low pH and temperature, the Raman spectrum shown in figure B1 and SEM images shown in figure 4.13 were used to identify the different phases. While most phases were identified using XRD, sample K:Nb-2.5-150 was not easily identified by its diffractogram. The XRD pattern does not fit well to any of the diffractograms of phases previously looked at and was not found in the crystallography open database (COD). Through SEM and Raman spectroscopy the three main potential phases found were $\text{K}_7\text{HfNb}_6\text{O}_{19} \cdot 13\text{H}_2\text{O}$, pyrochlore $\text{K}_2\text{Nb}_2\text{O}_6$ and $\text{K}_2\text{Nb}_2\text{O}_6 \cdot \text{H}_2\text{O}$. The SEM images, shown in figure 4.13c and 5.2, show large agglomerated crystals along with small fibers of less than 1 μm diameter length. These fibers are the most common morphology of the SOMS structure $\text{K}_2\text{Nb}_2\text{O}_6 \cdot \text{H}_2\text{O}$. $\text{Na}_2\text{Nb}_2\text{O}_6 \cdot \text{H}_2\text{O}$ has this fibrous morphology, and have similar crystal structure and unit cell as $\text{K}_2\text{Nb}_2\text{O}_6 \cdot \text{H}_2\text{O}$. The Raman spectrum show that the K:Nb-2.5-150 sample has the same bands as the $\text{K}_7\text{HfNb}_6\text{O}_{19} \cdot 13\text{H}_2\text{O}$ phase at $\sim 225, 290, 530, 840$ and 890 cm^{-1} . The Raman spectra for $\text{K}_2\text{Nb}_2\text{O}_6 \cdot \text{H}_2\text{O}$ has the same main bands as $\text{K}_7\text{HfNb}_6\text{O}_{19} \cdot \text{H}_2\text{O}$ at 225, 290, 840 and 890 so this is unhelpful in differentiating the two phases. In the full Raman spectrum shown in Appendix B1, $\text{K}_7\text{HfNb}_6\text{O}_{19} \cdot 13\text{H}_2\text{O}$ has a noticeable band at $\sim 3000\text{-}3600\text{ cm}^{-1}$ which represents the OH bond stretching from the crystal water. The Raman spectrum for K:Nb-2.5-150 does not have a band at this range of wavenumbers, which could indicate the sample has less crystal water.

The XRD pattern of K:Nb-2.5-150, shown in figure 5.1, remains unidentified. If the sample contains $\text{K}_7\text{HfNb}_6\text{O}_{19} \cdot 13\text{H}_2\text{O}$, the XRD pattern does not match the monoclinic structure with the space group P21. A potential reason the XRD pattern is not the same as the monoclinic P21 $\text{K}_7\text{HfNb}_6\text{O}_{19} \cdot 13\text{H}_2\text{O}$ patterns could be because of a difference in crystal water amount or a different space group. Another possibility would be that the agglomerated phase that does not have the fiber structure is $\text{K}_2\text{Nb}_2\text{O}_6$ but with the pyrochlore type structure instead of the SOMS structure of the $\text{K}_2\text{Nb}_2\text{O}_6 \cdot \text{H}_2\text{O}$ fibers [?, ?]. If that is the case, the sample largely consists of $\text{K}_2\text{Nb}_2\text{O}_6 \cdot x\text{H}_2\text{O}$ ($x=0\text{-}1$). Without proper identification of the XRD pattern the exact identity of the sample remains uncertain. There might be a small amount of $\text{K}_4\text{Nb}_6\text{O}_{17}$ with plate morphology as well, perhaps visible in the XRD pattern and in the SEM images, but this is not confirmed.

5.2.2 $\text{K}_4\text{Nb}_6\text{O}_{17}$ Diffractogram and Degree of Hydration

From the X-ray diffractogram of the three $\text{K}_4\text{Nb}_6\text{O}_{17}$ samples it is clear that some peaks are broad and weak while some are sharper and more intense. Generally when the crystallite size is on the nanoscale the diffraction lines broaden and becomes less intense. If a particle has one or more nanosized dimensions, such as the nanometer sized thickness of the $\text{K}_4\text{Nb}_6\text{O}_{17}$ nano plates, seen in figure 4.13d), while other dimensions are of micrometer scale, the diffractogram will have these selective peak features. The $\text{K}_4\text{Nb}_6\text{O}_{17}$ nano plates studied are $\sim 1\text{ }\mu\text{m}$ wide and long, but only a few *nm* thick. The crystallographic planes that run perpendicular to the plate will

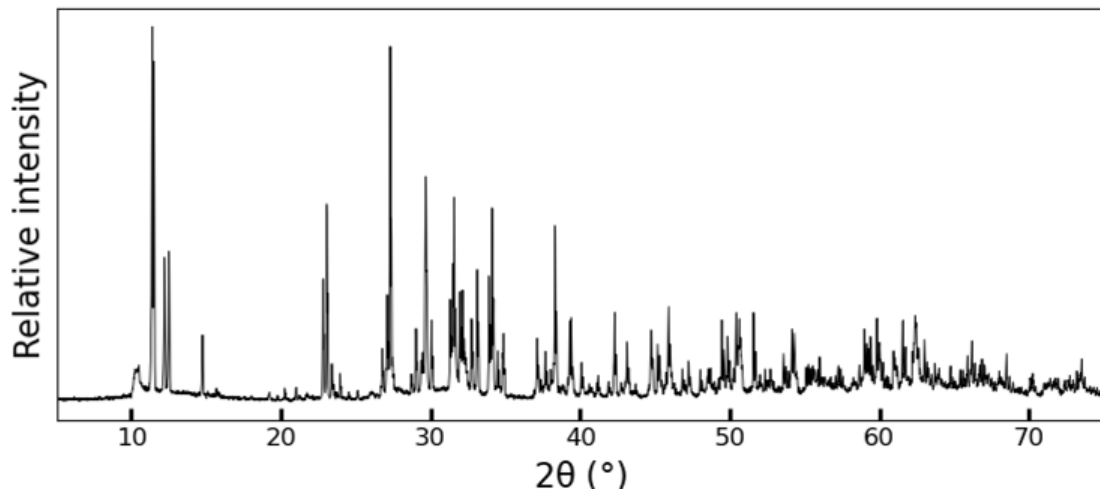


Figure 5.1: XRD pattern of the K:Nb-2.5-150 sample, which was identified using Raman spectroscopy and SEM to contain $\text{K}_7\text{HNb}_6\text{O}_{19} \cdot 13\text{H}_2\text{O}$ & $\text{K}_2\text{Nb}_2\text{O}_6 \cdot \text{H}_2\text{O}$.

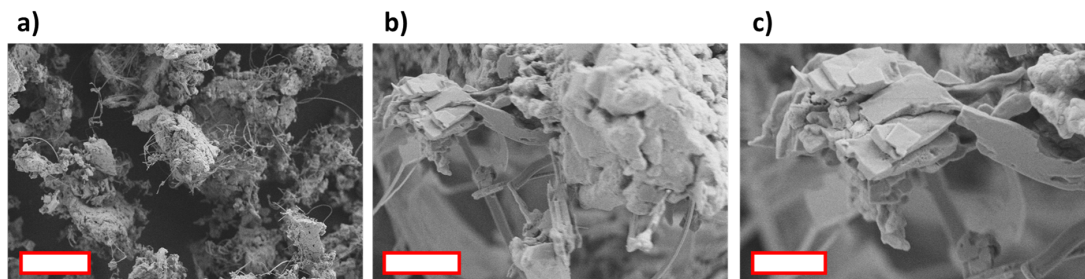


Figure 5.2: SEM images of sample K:Nb-2.5-150 with scale bars showing **a)** 40 μm , **b)** 4 μm and **c)** 2 μm . While zoomed out the fibers are visible throughout the structure, and when zoomed in both the $\text{K}_2\text{Nb}_2\text{O}_6 \cdot \text{H}_2\text{O}$ fibers and some plates are visible on an agglomerated phase similar to the $\text{K}_7\text{HNb}_6\text{O}_{19} \cdot 13\text{H}_2\text{O}$ phase. The plates could be the $\text{K}_4\text{Nb}_6\text{O}_{17}$ phase, which has a plate morphology, but this cannot be confirmed by the SEM images alone.

give broad and less intense diffraction lines while the planes running parallel to the plate direction will make the diffraction lines sharper and more intense. The peak at $9.3^\circ 2\theta$ of the $\text{K}_4\text{Nb}_6\text{O}_{17}$ diffractogram corresponds to the (040) plane and the peak at $27.8^\circ 2\theta$ to the (270) plane [34, 62]. A large overlap of all the low intensity broad diffraction lines makes Rietveld refinement less accurate.

The degree of hydration of $\text{K}_4\text{Nb}_6\text{O}_{17}$ can be assessed using Raman spectroscopy by looking at the region of the Raman spectrum between 3000 and 3600 cm^{-1} where the OH bands appear. The Raman spectrum for $\text{K}_4\text{Nb}_6\text{O}_{17}$ does not show a significant OH band, meaning the compound is mostly dehydrated. A thermogravimetric analysis would show more information on the hydration degree but was not carried out in this project.

5.2.3 Solution Behavior at 5 M KOH

The samples made at 5 M KOH had interesting solution behavior. K:Nb-5-200 was produced twice because the first attempted experiment yielded KNbO_3 which was unexpected because the sample made with the same temperature but 7.5 M KOH produced $\text{K}_7\text{HfNb}_6\text{O}_{19} \cdot 10\text{H}_2\text{O}$. On the second attempt, the products of both K:Nb-5-200 and K:Nb-7.5-200 were $\text{K}_7\text{HfNb}_6\text{O}_{19} \cdot 10\text{H}_2\text{O}$. No other samples at 5 M KOH resulted in KNbO_3 , not even at 240 °C, which prompted this experiment to be redone. The reasons for the sample having enough energy to overcome the energy barrier and producing KNbO_3 are unknown and hard to investigate since the results were not reproducible.

Another observation is that all the controlled K:Nb experiments with 5 M KOH, with a 1.33 K:Nb molar ratio and only 1 mL KOH volume added, were clear solutions with no precipitate. For the constant niobium concentration experiments, with K:Nb molar ratio of 6.65 and 5 mL volume, two experiments gave clear solutions and three precipitated solids. Higher volume and a larger excess KOH made the solution conditions better for precipitation. Samples [Nb]-5-180 and [Nb]-5-240 contained no precipitate, the rest of the [Nb] experiments did. All the samples at higher and lower pH, both for sodium and potassium, had solid precipitate.

5.3 Monoclinic KNbO_3

To distinguish the two crystal structures of KNbO_3 , monoclinic and orthorhombic, a few special features in the XRD pattern shown in figure 5.3 and Raman spectra must be looked at. The two phases are almost identical except the β angle for the monoclinic phase is not 90 °. The difference however, is small; Rietveld refinement gave a β angle between 89.9 and 90.1 °. In the diffractogram for monoclinic KNbO_3 most of the diffraction lines are broader with slight differences in the intensity of the diffraction lines as seen in figure 5.3a). This is especially apparent in the peaks around 45 ° 2θ as shown in figure 5.3b).

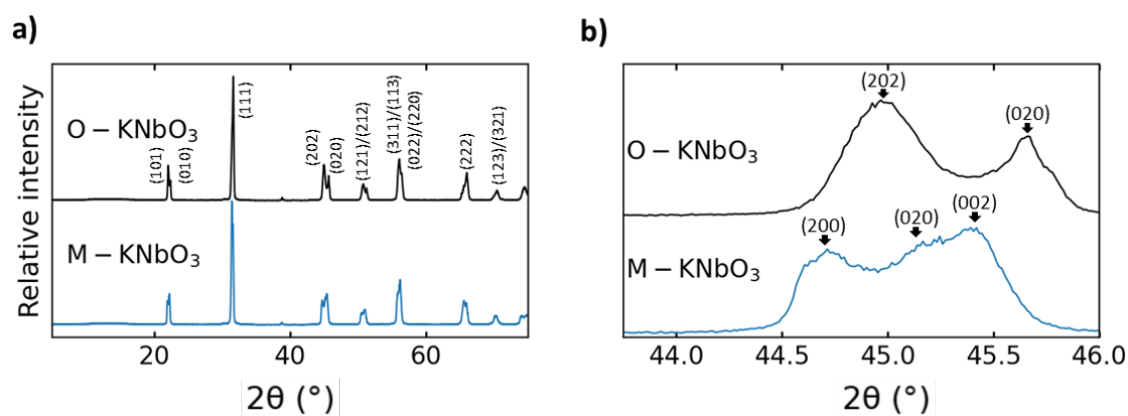


Figure 5.3: a) XRD pattern of monoclinic and orthorhombic KNbO_3 , b) zoomed in on the area between 44 and 46 ° 2θ . here are differences despite the overall similarity of the spectra.

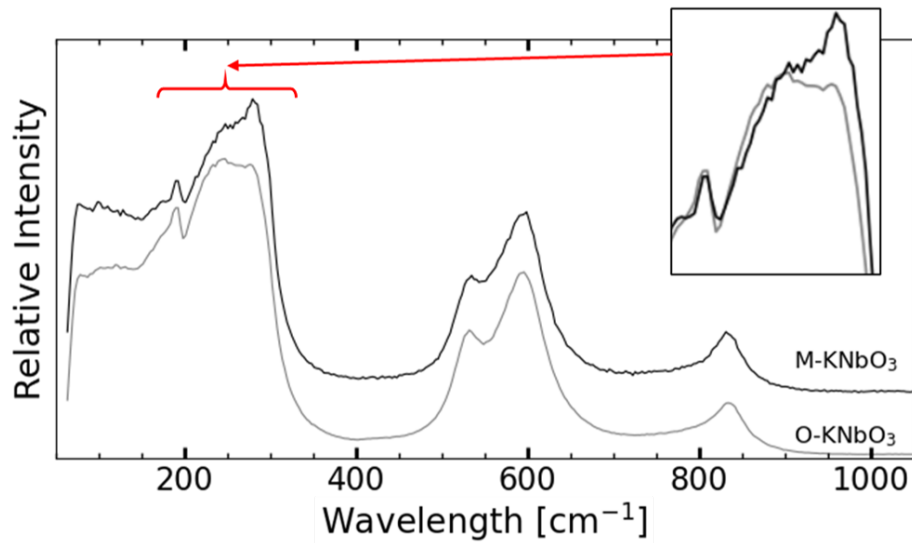


Figure 5.4: Raman spectra of orthorhombic (gray) and monoclinic (black) KNbO_3 . The spectra are overlapped and zoomed in the $150\text{-}300\text{ cm}^{-1}$ range to show the difference. Monoclinic KNbO_3 has an extra tall band at 280 cm^{-1} .

The Raman spectra of the monoclinic and orthorhombic KNbO_3 samples are shown in figure 5.4. The spectra are almost identical, the main difference being the band at 280 cm^{-1} where the monoclinic KNbO_3 has a sharper "bump" to the band compared to orthorhombic KNbO_3 . The local structure of orthorhombic and monoclinic KNbO_3 are almost identical, the increase in intensity at 280 cm^{-1} mean the Nb-O-Nb $A_1(\text{TO})$ and $A_1(\text{LO})$ modes are changed. Raman intensity is a function of bond polarizability and symmetry [63]. The monoclinic KNbO_3 has a difference in symmetry, and perhaps polarizability, caused by the change in β angle compared to orthorhombic KNbO_3 .

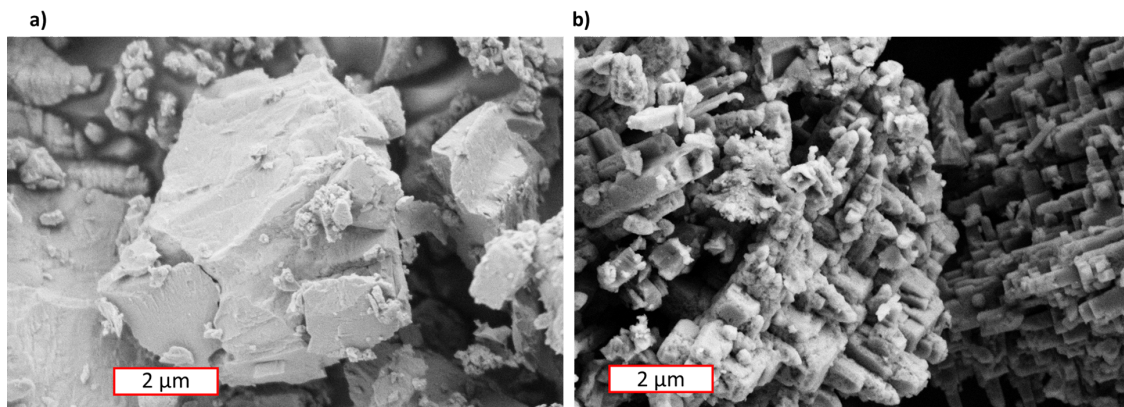


Figure 5.5: SEM images of a) orthorhombic and b) monoclinic KNbO_3 . The monoclinic phase was made at lower temperatures, between 165 and 200 degrees, while the orthorhombic phase was made at higher temperatures. The crystals of the orthorhombic phase does not have a regular morphology, while the crystals of the monoclinic phase have right rectangular prism morphology.

The SEM images of the monoclinic and the orthorhombic phases are shown in figure 5.5. The phases imaged have not been produced at the same temperature; the monoclinic phase was synthesized at 200 °C while the orthorhombic phase was synthesized at 240 °C. Higher temperatures lead to higher degrees of agglomeration, which is observed in the orthorhombic phase. The crystals in 5.5b) also show some agglomeration but the crystals have still retained the right rectangular prism morphology similar to NaNbO_3 .

The monoclinic phase was only produced at temperatures below 240 °C. A reason for this might be that the KNbO_3 has a tetragonal crystal structure above 224 °C. During synthesis at 240 °C the KNbO_3 product that has formed in the autoclave will have tetragonal crystal structure, when the autoclave is cooled down a phase change occurs. The tetragonal KNbO_3 transforms into the orthorhombic crystal structure, not monoclinic [64]. This phase transition at 224 °C does not seem like a viable synthesis route to monoclinic KNbO_3 . When no such phase transition occurs, the monoclinic KNbO_3 can form in the temperature region below 224 °C.

The exact mechanism for the formation of monoclinic KNbO_3 is not certain but some indications can be derived from this work. No monoclinic KNbO_3 was synthesized with the reaction conditions of the controlled K:Nb molar ratio experiments, even below 224 °C. The main difference in synthesis conditions between the controlled K:Nb experiments and the constant [Nb] experiments are shown in Table 3.2 and 3.3. More solution in the autoclave, which lead to a lower niobium concentration and increased K:Nb molar ratio, lead to the formation of monoclinic KNbO_3 . The constant [Nb] experiments had higher excess K^+ and a higher filling factor of $\sim 20\%$ as opposed to the K:Nb experiments which had $\sim 5\%$ filling factor and formed orthorhombic KNbO_3 . Higher volume could mean a somewhat increased pressure at these temperatures.

5.4 Formation Mechanisms of Alkali Niobates

The formation mechanism for alkali niobates, especially $(\text{K}, \text{Na})\text{NbO}_3$, has been studied extensively to understand the $(\text{K}, \text{Na})\text{-Nb-O}$ system better. Knowledge on the intermediate phases and the reaction kinetics leads to better control over the synthesis and the properties of the final product. Figure 5.6 shows the proposed formation mechanism which builds on the work of this project as well as literature [17, 27, 29].

After dissolution of Nb_2O_5 the first phase to form is $(\text{K}, \text{Na})_{8-x}\text{H}_x\text{Nb}_6\text{O}_{19} \cdot n\text{H}_2\text{O}$. This is well understood in the literature and is the phase that forms at the lowest temperatures. It is also the phase that rapidly precipitates when the free niobate species in solution are mixed with ethanol. The phases that form after $(\text{K}, \text{Na})_{8-x}\text{H}_x\text{Nb}_6\text{O}_{19} \cdot n\text{H}_2\text{O}$ depends on the reaction conditions. At higher temperature but low concentration of KOH , the hexaniobate Lindqvist anion rearranges into edge shared units of $[\text{Nb}_6\text{O}_{17}]$, which are flatter and connect with other such units via corner shared octahedra. This forms sheets with potassium atoms in between, which grow preferentially along the sheet direction and gaining nanosheet morphology. At higher temperature and high

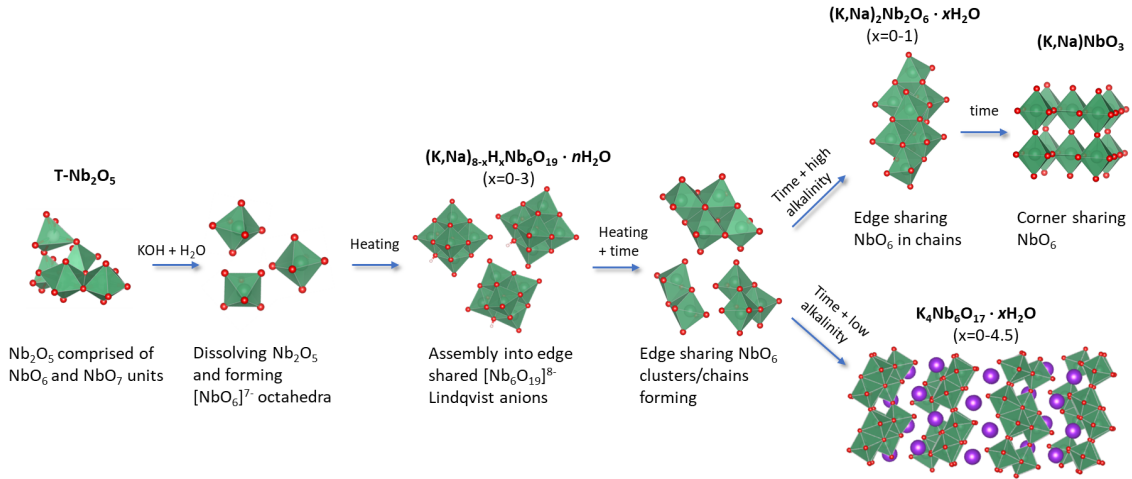


Figure 5.6: Proposed formation mechanism of alkali niobates such as $(\text{K,Na})\text{NbO}_3$ and $\text{K}_4\text{Nb}_6\text{O}_{17}$ based on the experimental evidence as well as literature [27, 29]. Nb_2O_5 dissolves, forming $[\text{NbO}_6]^{7-}$ units that assemble into the hexaniobate Lindqvist anion phase $(\text{K,Na})_{8-x}\text{H}_x\text{Nb}_6\text{O}_{19} \cdot n\text{H}_2\text{O}$ ($x=0-3$). The hexaniobate Lindqvist anion breaks up forming clusters and chains, higher alkalinity forming smaller clusters. At high alkalinity the smaller clusters link up into edge shared chains, which rearranges over time. First into edge shared and corner shared octahedra for the $(\text{K,Na})_2\text{Nb}_2\text{O}_6 \cdot \text{H}_2\text{O}$ and finally all corner shared octahedra in the $(\text{K,Na})\text{NbO}_3$ phase. At low alkalinity the clusters are not as small, and form $\text{K}_4\text{Nb}_6\text{O}_{17} \cdot x\text{H}_2\text{O}$.

$(\text{Na,K})\text{OH}$ concentration the hexaniobate Lindqvist anion break up even more, into smaller units such as $[\text{NbO}_6]^{7-}$ and $[\text{Nb}_2\text{O}_{10}]^{10-}$, which arrange themselves into chains to form $(\text{K,Na})_2\text{Nb}_2\text{O}_6 \cdot \text{H}_2\text{O}$ or directly into $(\text{K,Na})\text{NbO}_3$ if the temperature and pH are high enough. $\text{K}_2\text{Nb}_2\text{O}_6 \cdot \text{H}_2\text{O}$ is metastable, and quickly reacts into KNbO_3 , while $\text{Na}_2\text{Nb}_2\text{O}_6 \cdot \text{H}_2\text{O}$ is more stable over a broader range of temperatures and NaOH concentrations.

6 Conclusion

Understanding the synthesis conditions and their effects on alkali niobates is important when looking to utilize the interesting properties of the different materials. The aim of the project was investigating different parameters effect on the synthesis of alkali niobates. The effect of temperature, alkalinity, K:Nb molar ratio and niobium concentration on the type of phase made and the lattice parameters were the main focus. The conclusions can be summarized with these six points:

- Temperature is the most important factor for reaction kinetics and overcoming energy barriers to form alkali niobates such as $(\text{K}, \text{Na})\text{NbO}_3$ and $\text{K}_4\text{Nb}_6\text{O}_{17}$
- Alkalinity is the factor that helps select the alkali niobate phase, it determines which NbO_6 clusters are formed after the Lindqvist anion breaks down
- Higher K:Nb molar ratio and lower niobium concentration enables the formation KNbO_3 at lower KOH concentrations
- Monoclinic KNbO_3 , a metastable phase not previously synthesized using Nb_2O_5 as the precursor, forms at temperatures of 200 °C and below at 7.5-10 M KOH with high K:Nb molar ratio and low niobium concentration
- Sodium niobates have faster reaction kinetics and more uniform morphology than potassium niobates
- Crystallite size increases with higher temperatures, monoclinic KNbO_3 having larger crystallite size than orthorhombic KNbO_3

The improved understanding of the potassium and sodium niobate systems is another step towards biocompatible and environmentally friendly and cheap piezoelectric materials. The discovery of synthesis conditions that can produce monoclinic KNbO_3 using Nb_2O_5 instead of metallic niobium powder is a key development towards commercially viable functional potassium niobates.

7 Future Research

Further research can attempt to identify the crystal structure and space group of sample K:Nb-2.5-150. The XRD pattern was not identified, but was highly crystalline. The Raman spectrum was very similar to the spectra for the $\text{K}_7\text{HfNb}_6\text{O}_{19} \cdot 13\text{H}_2\text{O}$ samples, making it likely that this sample is either $\text{K}_7\text{HfNb}_6\text{O}_{19} \cdot 13\text{H}_2\text{O}$ with a different crystal structure and space group or a different material entirely, for example pyrochlore $\text{K}_2\text{Nb}_2\text{O}_6$. Sample [Nb]-7.5-180 was a multi-phase material with unidentified peaks in the XRD spectrum. Looking at this sample in the SEM was not done in this project, but could reveal interesting morphology and help identify phases.

Investigating the monoclinic KNbO_3 might lead to interesting properties that have technological uses. Monoclinic KNbO_3 synthesized using Nb_2O_5 as the precursor could potentially have better functional properties as opposed to the samples made from niobium metal powder. Functional properties such as optical properties and intensity of second harmonic generation are of interest [64].

Sodium niobates were not investigated much in this study, the 6 samples made were useful for comparison of the reaction kinetics. Further study of sodium niobates made at low temperature and low NaOH concentration would reveal information on the sodium niobate reaction kinetics and phases. Time is also a factor that can be varied to study different sodium niobate phases produced before NaNbO_3 . With slower kinetics, at lower temperatures, NaOH concentration and shorter reaction time, different sodium niobate phases can be studied.

A 2014 study reported the preparation of $\text{K}_2\text{Nb}_2\text{O}_6$ with cubic pyrochlore structure made at 3 M KOH and 240 °C [37]. Pyrochlore $\text{K}_2\text{Nb}_2\text{O}_6$ was not formed at 2.5 or 5 M KOH and 240 °C in this work. Investigating the synthesis conditions that produced this phase can be important for controlling properties of KNbO_3 . $\text{K}_2\text{Nb}_2\text{O}_6$ is a known precursor phase to KNbO_3 , creating a structure that is slightly different to KNbO_3 produced directly by hydrothermal synthesis [17]. Understanding $\text{K}_2\text{Nb}_2\text{O}_6$, the crystal structure, XRD pattern and Raman spectrum, will help identify the XRD pattern for sample K:Nb-2.5-150.

8 References

- [1] Alexander H. King. Our elemental footprint. *Nature Materials*, 18(5):408–409, May 2019.
- [2] Eiichi Fukada and Iwao Yasuda. On the piezoelectric effect of bone. *Journal of the Physical Society of Japan*, 12(10):1158–1162, 1957.
- [3] Adrian Demayo, Margaret C. Taylor, Kenneth W. Taylor, Peter V. Hodson, and Paul B. Hammond. Toxic effects of lead and lead compounds on human health, aquatic life, wildlife plants, and livestock. *C R C Critical Reviews in Environmental Control*, 12(4):257–305, 1982.
- [4] Ab Latif Wani, Anjum Ara, and Jawed Ahmad Usmani. Lead toxicity: a review. *Interdisciplinary toxicology*, 8(2):55–64, June 2015.
- [5] Shujun Zhang, Ru Xia, and Thomas R. ShROUT. Lead-free piezoelectric ceramics vs. pzt? *Journal of Electroceramics*, 19(4):251–257, Dec 2007.
- [6] Kunzhan Cai, Yilai Jiao, Quan Quan, Yulin Hao, Jie Liu, and Lin Wu. Improved activity of mc3t3-e1 cells by the exciting piezoelectric BaTiO₃/tc4 using low-intensity pulsed ultrasound. *Bioactive Materials*, 6(11):4073–4082, 2021.
- [7] Kangqi Fan, Jianwei Chang, Fengbo Chao, and Witold Pedrycz. Design and development of a multipurpose piezoelectric energy harvester. *Energy Conversion and Management*, 96:430–439, 2015.
- [8] Shujun Zhang and Fapeng Yu. Piezoelectric materials for high temperature sensors. *Journal of the American Ceramic Society*, 94(10):3153–3170, 2011.
- [9] Xiangyu Gao, Jikun Yang, Jingen Wu, Xudong Xin, Zhanmiao Li, Xiaoting Yuan, Xinyi Shen, and Shuxiang Dong. Piezoelectric actuators and motors: Materials, designs, and applications. *Advanced Materials Technologies*, 5(1):1900716, 2020.
- [10] Jih Mirn Jehng and Israel E. Wachs. Structural chemistry and raman spectra of niobium oxides. *Chemistry of Materials*, 3(1):100–107, Jan 1991.
- [11] Izabela Nowak and Maria Ziolk. Niobium compounds: Preparation, characterization, and application in heterogeneous catalysis. *Chemical Reviews*, 99(12):3603–3624, 1999.
- [12] Jiagang Wu, Dingquan Xiao, and Jianguo Zhu. Potassium–sodium niobate lead-free piezoelectric materials: Past, present, and future of phase boundaries. *Chemical Reviews*, 115(7):2559–2595, 2015. PMID: 25792114.
- [13] May Nyman. Polyoxoniobate chemistry in the 21st century. *Dalton Trans.*, 40:8049–8058, 2011.

- [14] Gauthier J.-P. Deblonde, Alexandre Chagnes, Sarah Bélair, and Gérard Cote. Solubility of niobium(v) and tantalum(v) under mild alkaline conditions. *Hydrometallurgy*, 156:99–106, 2015.
- [15] Jih-Mirn Jehng and Israel E. Wachs. Niobium oxide solution chemistry. *Journal of Raman Spectroscopy*, 22(2):83–89, 1991.
- [16] May Nyman, Aaron J. Celestian, John B. Parise, Gregory P. Holland, and Todd M. Alam. Solid-state structural characterization of a rigid framework of lacunary heteropolyniobates. *Inorganic Chemistry*, 45(3):1043–1052, 2006.
- [17] Xingang Kong, Dengwei Hu, Puhong Wen, Tomohiko Ishii, Yasuhiro Tanaka, and Qi Feng. Transformation of potassium lindquist hexaniobate to various potassium niobates: solvothermal synthesis and structural evolution mechanism. *Dalton Trans.*, 42:7699–7709, 2013.
- [18] M. Filowitz, R. K. C. Ho, W. G. Klemperer, and W. Shum. ^{17}O nuclear magnetic resonance spectroscopy of polyoxometalates. 1. sensitivity and resolution. *Inorganic chemistry*, 18(1):93–103, 1978.
- [19] Mari-Ann Einarsrud and Tor Grande. 1d oxide nanostructures from chemical solutions. *Chem. Soc. Rev.*, 43:2187–2199, 2014.
- [20] S.-H. Feng and G.-H. Li. Chapter 4 - hydrothermal and solvothermal syntheses. In Ruren Xu and Yan Xu, editors, *Modern Inorganic Synthetic Chemistry (Second Edition)*, pages 73–104. Elsevier, Amsterdam, second edition edition, 2017.
- [21] Shing Bo Peh and Dan Zhao. 1 - synthesis and development of metal–organic frameworks. In Jian Liu and Frank Ding, editors, *Nanoporous Materials for Molecule Separation and Conversion*, Micro and Nano Technologies, pages 3–43. Elsevier, 2020.
- [22] Richard I. Walton. Subcritical solvothermal synthesis of condensed inorganic materials. *Chem. Soc. Rev.*, 31:230–238, 2002.
- [23] Hong ming Zhou, Dan qing Yi, Yi Zhang, and Shi li Zheng. The dissolution behavior of Nb_2O_5 , Ta_2O_5 and their mixture in highly concentrated KOH solution. *Hydrometallurgy*, 80(1):126–131, 2005.
- [24] Satoshi Uchida, Yuichi Inoue, Yoshinobu Fujishiro, and Tsugio Sato. Hydrothermal synthesis of $\text{K}_4\text{Nb}_6\text{O}_{17}$. *Journal of Materials Science*, 33(21):5125–5129, Nov 1998.
- [25] Guodong Shi, Junhan Wang, Hengli Wang, Zhanjun Wu, and Huaping Wu. Hydrothermal synthesis of morphology-controlled KNbO_3 , NaNbO_3 , and $(\text{K}, \text{Na})\text{NbO}_3$ powders. *Ceramics International*, 43(9):7222–7230, 2017.

- [26] Gregory K. L. Goh, Fred F. Lange, Sossina M. Haile, and Carlos G. Levi. Hydrothermal synthesis of KNbO_3 and NaNbO_3 powders. *Journal of Materials Research*, 18(2):338–345, Feb 2003.
- [27] Susanne Linn Skjærvø, Sanna Sommer, Peter Nørby, Espen Drath Bøjesen, Tor Grande, Bo B. Iversen, and Mari-Ann Einarsrud. Formation mechanism and growth of MNbO_3 , $m=k$, na by in situ x-ray diffraction. *Journal of the American Ceramic Society*, 100(9):3835–3842, 2017.
- [28] Yuli Ma, Xiaoqing Liu, Yang Li, Yiguo Su, Zhanli Chai, and Xiaojing Wang. $\text{K}_4\text{Nb}_6\text{O}_{17} \cdot 4.5\text{H}_2\text{O}$: A novel dual functional material with quick photoreduction of Cr(VI) and high adsorptive capacity of Cr(III) . *Journal of Hazardous Materials*, 279:537–545, 2014.
- [29] Susanne Linn Skjærvø, Gary K. Ong, Ola Gjønnnes Grendal, Kristin Høydalsvik Wells, Wouter van Beek, Koji Ohara, Delia J. Milliron, Satoshi Tominaka, Tor Grande, and Mari-Ann Einarsrud. Understanding the hydrothermal formation of NaNbO_3 : Its full reaction scheme and kinetics. *Inorganic Chemistry*, 60(11):7632–7640, 2021. PMID: 33754706.
- [30] Ni Zhen, Jing Dong, Zhengguo Lin, Xiaoxia Li, Yingnan Chi, and Changwen Hu. Self-assembly of polyoxovanadate-capped polyoxoniobates and their catalytic decontamination of sulfur mustard simulants. *Chem. Commun.*, 56:13967–13970, 2020.
- [31] Miloslav Pekař. Thermodynamic driving forces and chemical reaction fluxes; reflections on the steady state. *Molecules (Basel, Switzerland)*, 25(3):699, Feb 2020.
- [32] Kent J. Griffith, Alexander C. Forse, John M. Griffin, and Clare P. Grey. High-rate intercalation without nanostructuring in metastable Nb_2O_5 bronze phases. *Journal of the American Chemical Society*, 138(28):8888–8899, 2016. PMID: 27264849.
- [33] May Nyman, Todd M. Alam, François Bonhomme, Mark A. Rodriguez, Colleen S. Frazer, and Margaret E. Welk. Solid-state structures and solution behavior of alkali salts of the $[\text{Nb}_6\text{O}_{19}]^{8-}$ lindqvist ion. *Journal of Cluster Science*, 17(2):197–219, Jun 2006.
- [34] Jin Sun, Dongjiang Yang, Cuihua Sun, Long Liu, Yang Shuanglei, Yi Jia, Rongsheng Cai, and X. Yao. Potassium niobate nanolamina: A promising adsorbent for entrapment of radioactive cations from water. *Scientific Reports*, 4:7313, 01 2014.
- [35] Chao Liu, Yue Feng, Zitong Han, Yao Sun, Xiaoqiu Wang, Qinfang Zhang, and Zhigang Zou. Z-scheme n-doped $\text{K}_4\text{Nb}_6\text{O}_{17}/\text{g-C}_3\text{N}_4$ heterojunction with superior visible-light-driven photocatalytic activity for organic pollutant removal and hydrogen production. *Chinese Journal of Catalysis*, 42(1):164–174, 2021.

- [36] Hongwu Xu, May Nyman, Tina M. Nenoff, and Alexandra Navrotsky. Prototype sandia octahedral molecular sieve (soms) $\text{Na}_2\text{Nb}_2\text{O}_6 \cdot \text{H}_2\text{O}$: Synthesis, structure and thermodynamic stability. *Chemistry of Materials*, 16(10):2034–2040, 2004.
- [37] Jingjing Wu, Chao Zhou, Yufei Zhao, Lu Shang, Tong Bian, Lei Shao, Feng Shi, Li-Zhu Wu, Chen-Ho Tung, and Tierui Zhang. One-pot hydrothermal synthesis and photocatalytic hydrogen evolution of pyrochlore type $\text{K}_2\text{Nb}_2\text{O}_6$. *Chinese Journal of Chemistry*, 32(6):485–490, 2014.
- [38] Woong-Hee Lee, Young-Jin Ko, Mir Im, Sang-Hyo Kweon, Sung-Hoon Cho, HaiBo Xu, Chong-Yun Kang, and Sahn Nahm. Formation of a KNbO_3 single crystal using solvothermally synthesized $\text{K}_{2-m}\text{Nb}_2\text{O}_{6-m/2}$ pyrochlore phase. *Journal of Electroceramics*, 41(1):37–42, Dec 2018.
- [39] Subhabrata Chakraborty, Sudhir Kumar Ghosh, Gopes Chandra Das, and Siddhartha Mukherjee. Optimization of synthesis conditions of monoclinic potassium niobate (KNbO_3) and its effect on morphology. *International Journal of Applied Ceramic Technology*, 13(4):743–752, 2016.
- [40] Seungwook Kim, Ju-Hyuck Lee, Jaeyeon Lee, Sang-Woo Kim, Myung Hwa Kim, Sungnam Park, Haegeun Chung, Yong-Il Kim, and Woong Kim. Synthesis of monoclinic potassium niobate nanowires that are stable at room temperature. *Journal of the American Chemical Society*, 135(1):6–9, 2013.
- [41] G. Shirane, H. Danner, A. Pavlovic, and R. Pepinsky. Phase transitions in ferroelectric KNbO_3 . *Phys. Rev.*, 93:672–673, Feb 1954.
- [42] Ken ichi Kakimoto, Shinro Ito, Izumi Masuda, and Hitoshi Ohsato. Growth morphology and crystal orientation of KNbO_3 film on SrTiO_3 by liquid phase epitaxy. *Japanese Journal of Applied Physics*, 41(Part 1, No. 11B):6908–6911, nov 2002.
- [43] Tommy Mokkalbost, Øystein Andersen, Ruth Astrid Strøm, Kjell Wiik, Tor Grande, and Mari-Ann Einarsrud. High-temperature proton-conducting LaNbO_4 -based materials: Powder synthesis by spray pyrolysis. *Journal of the American Ceramic Society*, 90(11):3395–3400, 2007.
- [44] J. Perl, J. Shin, J. Schümann, B. Faddegon, and H. Paganetti. Topas: An innovative proton monte carlo platform for research and clinical applications. *Medical Physics*, 39(11):6818–6837, 2012.
- [45] B. Faddegon, J. Ramos-Mendez, J. Schuemann, A. McNamara, J. Shin, J. Perl, and Paganetti H. The TOPAS Tool for Particle Simulation, a Monte Carlo Simulation Tool for Physics, Biology and Clinical Research. *Physica Medica*, 2020.
- [46] P. Vlazan, P. Sfirloaga, M. Poienar, and M. Stoia. Structure and properties of nanocrystalline Bi^{3+} doped KNbO_3 ceramics obtained by hydrothermal

- method. *Materials Today: Proceedings*, 4(7, Part 1):7018–7024, 2017. 13th International Conference on Nanosciences Nanotechnologies (NN16), July (5-8) 2016, Thessaloniki, Greece.
- [47] Stacy Gates-Rector and Thomas Blanton. The powder diffraction file: a quality materials characterization database. *Powder Diffraction*, 34(4):352–360, 2019.
- [48] Shaozheng Ji, Hong Liu, Yuanhua Sang, Wei Liu, Guangwei Yu, and Yanhua Leng. Synthesis, structure, and piezoelectric properties of ferroelectric and antiferroelectric NaNbO_3 nanostructures. *CrystEngComm*, 16, 07 2014.
- [49] M. Maczka, M. Ptak, A. Majchrowski, and J. Hanuza. Raman and ir spectra of $\text{K}_4\text{Nb}_6\text{O}_{17}$ and $\text{K}_4\text{Nb}_6\text{O}_{17} \cdot 3\text{H}_2\text{O}$ single crystals. *Journal of Raman Spectroscopy*, 42(2):209–213, 2011.
- [50] Jingyang Niu, Pengtao Ma, Hongyu Niu, Jie Li, Junwei Zhao, You Song, and Jingping Wang. Giant polyniobate clusters based on $[\text{Nb}_7\text{O}_{22}]^9$ units derived from a Nb_6O_{19} precursor. *Chemistry – A European Journal*, 13(31):8739–8748, 2007.
- [51] Hannah T. Kreissl, Molly M. J. Li, Yung-Kang Peng, Keizo Nakagawa, Thomas J. N. Hooper, John V. Hanna, Ashley Shepherd, Tai-Sing Wu, Yun-Liang Soo, and S. C. Edman Tsang. Structural studies of bulk to nanosize niobium oxides with correlation to their acidity. *Journal of the American Chemical Society*, 139(36):12670–12680, Sep 2017.
- [52] Ranko P. Bontchev and May Nyman. Evolution of polyoxoniobate cluster anions. *Angewandte Chemie International Edition*, 45(40):6670–6672, 2006.
- [53] X.B. Wang, Z.X. Shen, Z.P. Hu, L. Qin, S.H. Tang, and M.H. Kuok. High temperature raman study of phase transitions in antiferroelectric NaNbO_3 . *Journal of Molecular Structure*, 385(1):1–6, 1996.
- [54] R. J. C. Lima, W. Paraguassu, P. T. C. Freire, J. M. Sasaki, F. E. A. Melo, J. Mendes Filho, and S. Lanfredi. Temperature-dependent raman spectra of $\text{K}_{0.2}\text{Na}_{0.8}\text{NbO}_3$ ceramics. *Journal of Raman Spectroscopy*, 36(1):28–32, 2005.
- [55] Roberta Brayner and François Bozon-Verduraz. Niobium pentoxide prepared by soft chemical routes: morphology, structure, defects and quantum size effect. *Phys. Chem. Chem. Phys.*, 5:1457–1466, 2003.
- [56] Dongchang Chen, Jeng-Han Wang, Tsung-Fu Chou, Bote Zhao, Mostafa A. El-Sayed, and Meilin Liu. Unraveling the nature of anomalously fast energy storage in t- Nb_2O_5 . *Journal of the American Chemical Society*, 139(20):7071–7081, 2017.
- [57] K. Bormanis, M. Palatnikov, O. Shcherbina, A. Frolov, P. Chufyrev, and N. Sidorov. Physical properties and structure of niobium pentoxide ceramics treated by concentrated light flow. *Integrated Ferroelectrics*, 123(1):137–143, 2011.

- [58] M. N. Palatnikov, N. V. Sidorov, N. N. Mel'nik, and V. T. Kalinnikov. Concentration phase transitions and structural disordering in the system of solid solutions $\text{Li}_x\text{Na}_{1-x}\text{Ta}_{0.1}\text{Nb}_{0.9}\text{O}_3$. *Journal of Applied Spectroscopy*, 68(4):642–648, Jul 2001.
- [59] M.P.F. Graça, A. Meireles, C. Nico, and M.A. Valente. Nb_2O_5 nanosize powders prepared by sol–gel – structure, morphology and dielectric properties. *Journal of Alloys and Compounds*, 553:177–182, 2013.
- [60] J S de Andrade, A G Pinheiro, I F Vasconcelos, J M Sasaki, J A C de Paiva, M A Valente, and A S B Sombra. Raman and infrared spectra of KNbO_3 in niobate glass-ceramics. *Journal of Physics: Condensed Matter*, 11(22):4451–4460, jan 1999.
- [61] Huaiyong Zhu, Zhanfeng Zheng, Xueping Gao, Yining Huang, Zhimin Yan, Jin Zou, Hongming Yin, Qingdi Zou, Scott H. Kable, Jincal Zhao, Yunfei Xi, Wayde N. Martens, and Ray L. Frost. Structural evolution in a hydrothermal reaction between Nb_2O_5 and NaOH solution: From Nb_2O_5 grains to microporous $\text{Na}_2\text{Nb}_2\text{O}_6 \cdot \frac{2}{3}\text{H}_2\text{O}$ fibers and NaNbO_3 cubes. *Journal of the American Chemical Society*, 128(7):2373–2384, 2006.
- [62] Yuli Ma, Xiaoqing Liu, Yang Li, Yiguo Su, Zhanli Chai, and Xiaojing Wang. $\text{K}_4\text{Nb}_6\text{O}_{17} \cdot 4.5\text{H}_2\text{O}$: A novel dual functional material with quick photoreduction of Cr(VI) and high adsorptive capacity of Cr(III) . *Journal of Hazardous Materials*, 279:537–545, 2014.
- [63] Ph. Colomban and A. Slodczyk. Raman intensity: An important tool in the study of nanomaterials and nanostructures. *Acta Physica Polonica A*, 116(1):7–12, 7 2009.
- [64] Seungwook Kim, Min-Seop Kim, Chiho Lee, Sungnam Park, Won Il Cho, and Woong Kim. Structure–property relationship of metastable monoclinic potassium niobate (KNbO_3) nanowires during phase transitions. *Journal of Alloys and Compounds*, 709:415–421, 2017.
- [65] Brian H. Toby and Robert B. Von Dreele. *GSAS-II*: the genesis of a modern open-source all purpose crystallography software package. *Journal of Applied Crystallography*, 46(2):544–549, Apr 2013.

Appendix

A X-Ray Diffraction Patterns

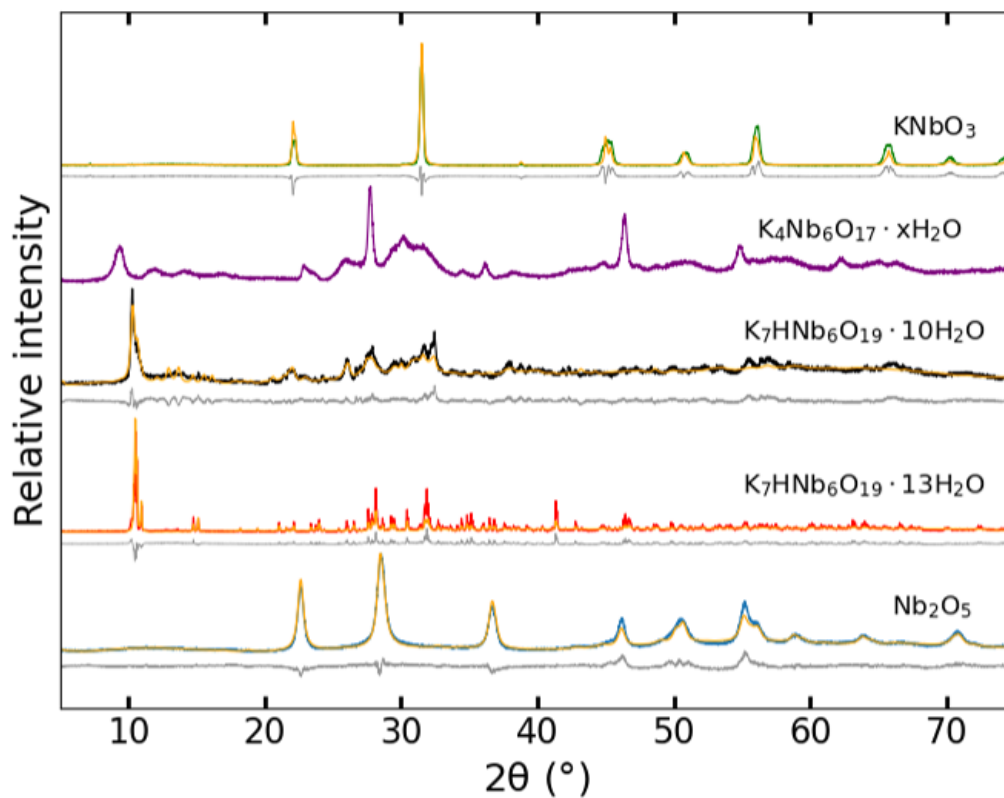


Figure A1: Example of the diffractogram pattern for the main potassium phases along with the calculated fit (orange) and the difference between the calculated fit and the raw data (gray).

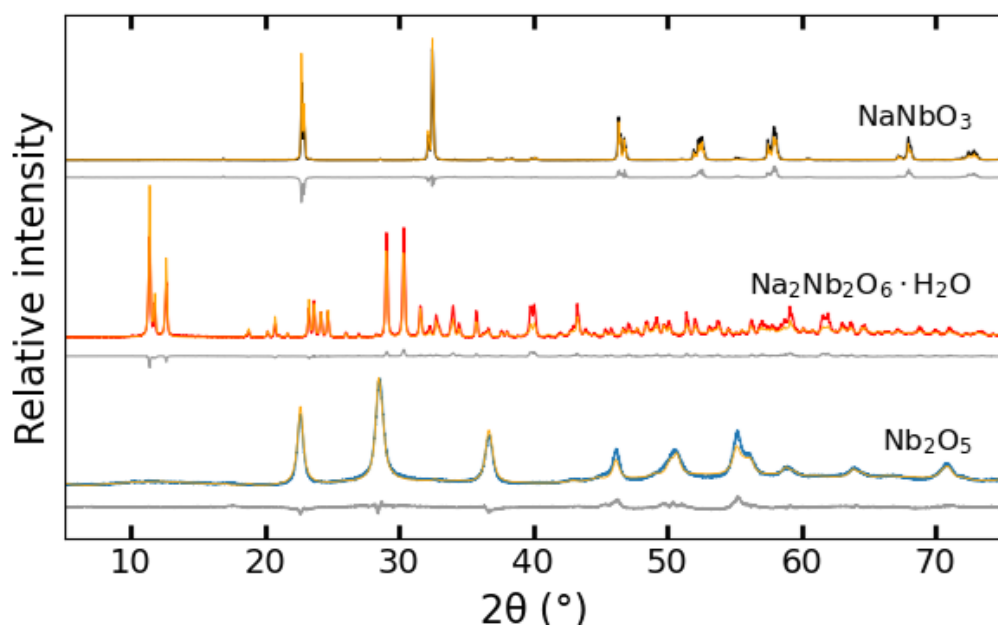


Figure A2: Example of the diffractogram pattern for the main sodium phases along with the calculated fit (orange) and the difference between the calculated fit and the raw data (gray).

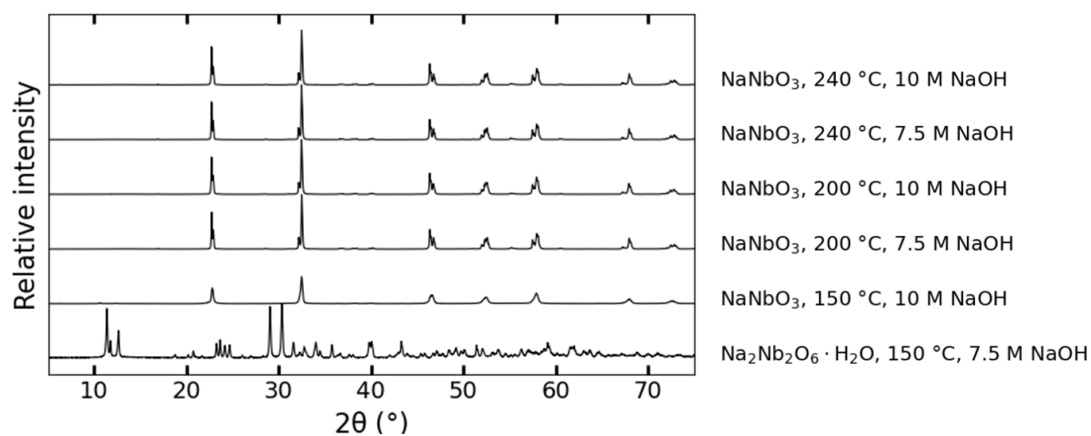


Figure A3: All the sodium niobate diffractogram patterns, shown in order of increasing temperature and pH from the bottom up.

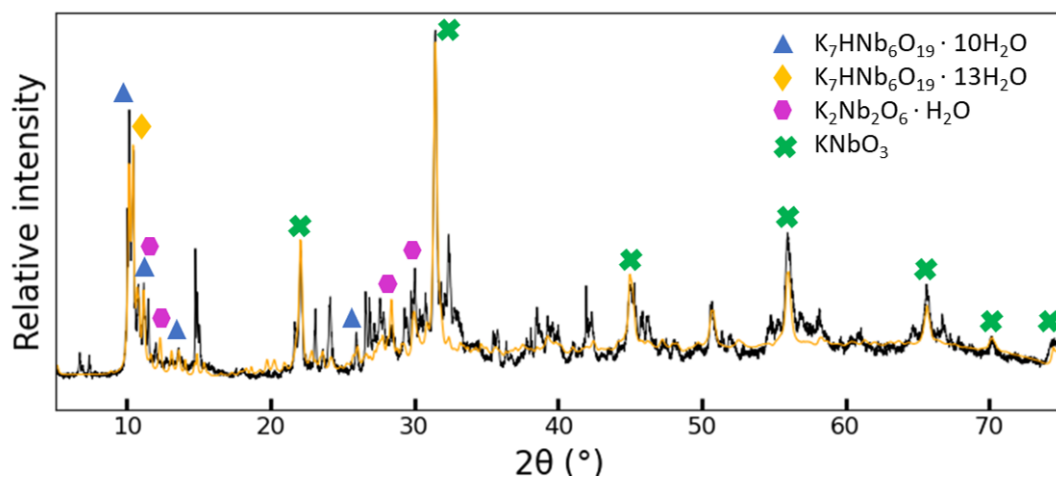


Figure A4: An example of a multi-phase material analyzed using TOPAS. The calculated fit, shown in orange, is not particularly accurate but the main diffraction lines of each phase are represented. Due to large overlap of the diffractogram, information such as the lattice parameters and exact phase composition is hard to acquire.

B Raman Spectroscopy

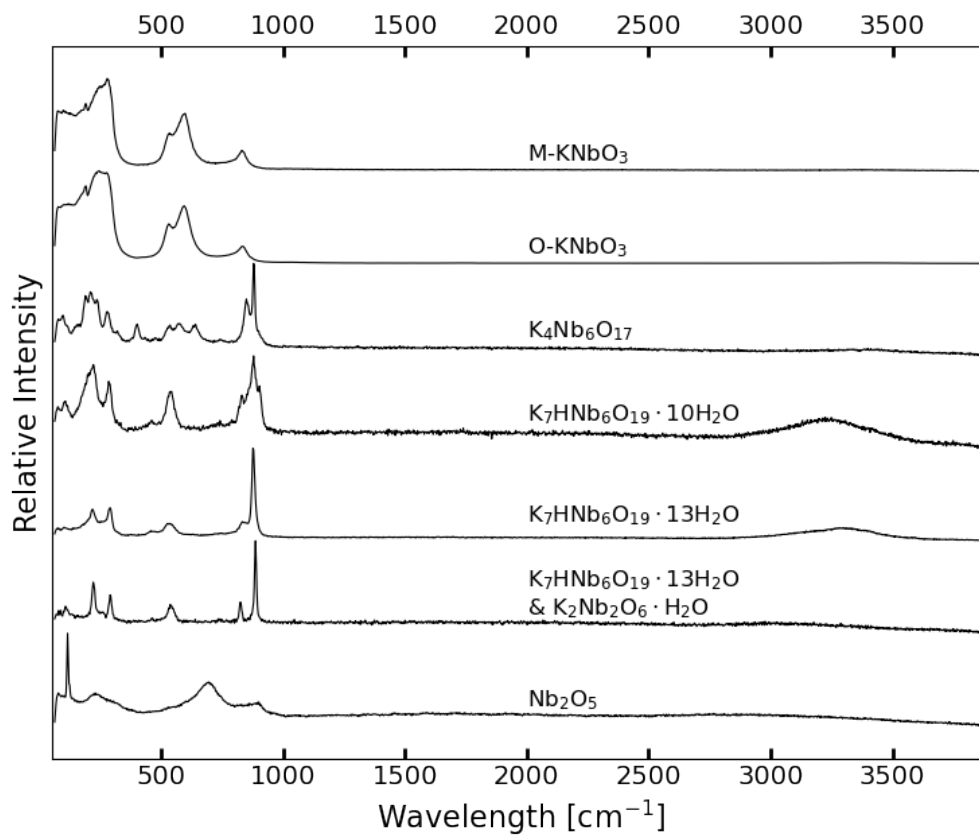


Figure B1: Full Raman spectrum for potassium niobates, showing the broad OH stretching band at 3000-3500 cm⁻¹ from the crystal water in some of the samples.

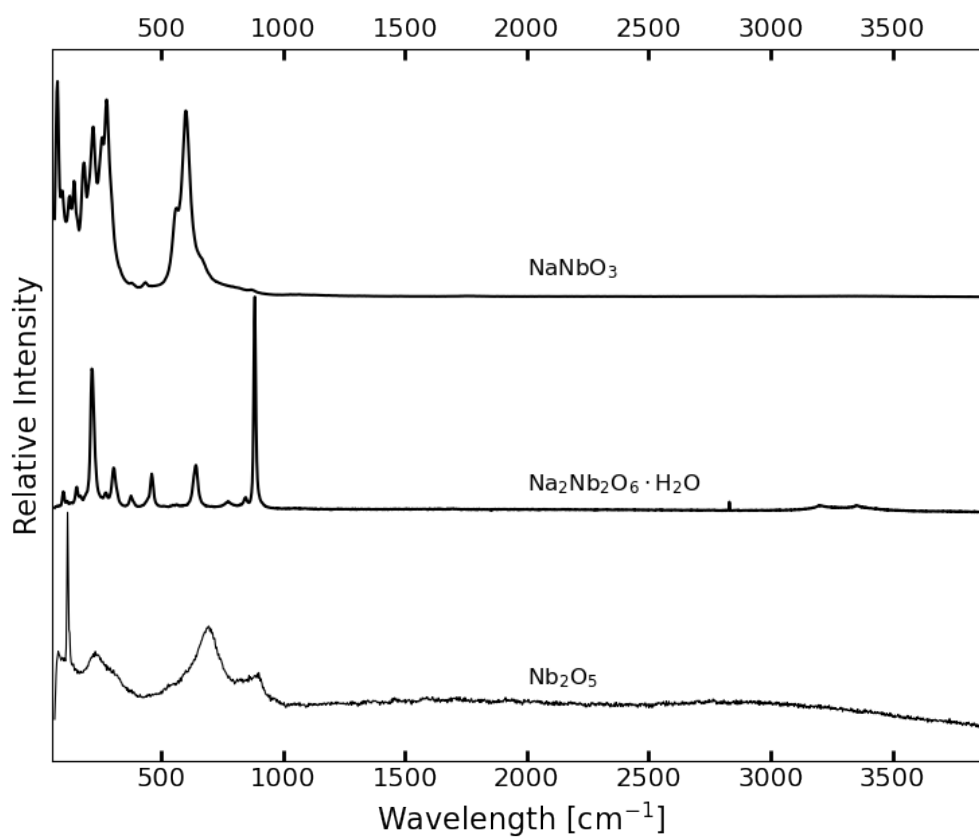


Figure B2: Full Raman spectrum for sodium niobates, showing the small OH stretching band at 3000-3500 cm⁻¹ from the crystal water in Na₂Nb₂O₆ · H₂O.

